united nations
educational, scientific
and cultural
organization

international atomic
energy agency

the
abdus salam
international centre for theoretical physics

SMR: 1133/10

WINTER COLLEGE ON
SPECTROSCOPY AND APPLICATIONS

(8 - 26 February 1999)

"Laser Diagnostics in Combustion Processess"

presented by:

Christof SCHULZ
Universität Heidelberg
Physikalisch-Chemisches Institut
Im Neuenheimer Feld 253
D-69120 Heidelberg
Germany

Twenty-Seventh Symposium (International) on Combustion/The Combustion Institute, 1998

HOTTEL PLENARY LECTURE

LASER IN COMBUSTION: FROM SIMPLE MODELS TO REAL DEVICES

Jürgen Wolfrum
Universität Heidelberg
Physikalisch-Chemisches Institut
Im Neuenheimer Feld 253
Heidelberg, Germany

Introduction

Electromagnetic radiation and combustion were always closely related. However, it took almost 1.6 million years, from the time the early homo erectus near Koobi Fora [1] (East Africa) enjoyed the heat, light and protection from wild animals by fire-generated radiation, until Hoyt Hottel [2] described quantitatively the heat transmission by radiation from non-luminous gases. Another important observation on radiation of hot gases from a combustion process was made in 1859 by the two Heidelberg scientists Robert Wilhelm Bunsen and Gustav Robert Kirchhoff [3] who recognized the origin of some of the famous dark lines in the solar spectrum first seen by Wollaston and indexed in 1814 by Josef Fraunhofer. Bunsen wrote the 15th November 1859 to his friend Henry Roscoe in England[4]: "At present Kirchhoff and I are occupied with a joint piece of work which will not let us sleep. Kirchhoff has made a wonderful, quite unexpected discovery, in that he has found the source of the dark lines in the sun's spectrum and has intensified these lines artificially and brought them out in the lineless spectrum, with the positions of the identical Frauenhofer lines. In this way the chemical composition of the sun and the fixed stars can be detected with the same certainty with which we determine sulphuric acid, chlorine, etc. with our reagents." Bunsen and Kirchhoff realized that it could not happen by chance that sixty of the Fraunhofer lines coincided with sixty iron emission lines measured in the hot non-luminous flame gases of the Bunsen burner. Their experimental success, however, was based on Isaac Newton, who introduced the word spectrum into physics and wrote in 1672 to the Royal Scientific Society about his observation that he could separate the colours of the sunlight by a prism. After Bunsen and Kirchhoff, spectroscopy in flames became a rapidly growing field. However, the meaning of all the observed lines was not known until 1913 when Niels Bohr formulated his model of the atom. A few years later in 1916 and 1917 Albert Einstein [5] published his famous paper "Zur Quantentheorie der Strahlung" in which he derived Planck's law and Bohr's rule by discussing the possible elementary process of energy and momentum exchange through radiation. He discovered that a consistent quantum theory can only be obtained by assuming that the radiative processes 'Ausstrahlung' (spontaneous emission) and 'Einstrahlung' (absorption and stimulated emission) are directed processes and, besides energy, also momentum exchange is taken into account. Despite Einstein's clear description of the stimulated emission, the practical realization of this principle was achieved only many years later in 1955, first in the microwave region (MASER) [6] and in 1960 the visible spectral region (LASER) [7]. It is interesting to note that the effect of stimulated emission had already been experimentally observed in 1928 by Hans Kopfermann in careful experiments on light dispersion around several neon lines. He established the existence of the negative absorption ending not far from the helium-sensitized neon gas laser [8]. As shown in Fig. 1, the principle of stimulated emission has now been realized in all states of the matter: solids, liquids, gases, and free electrons. This allows genera-

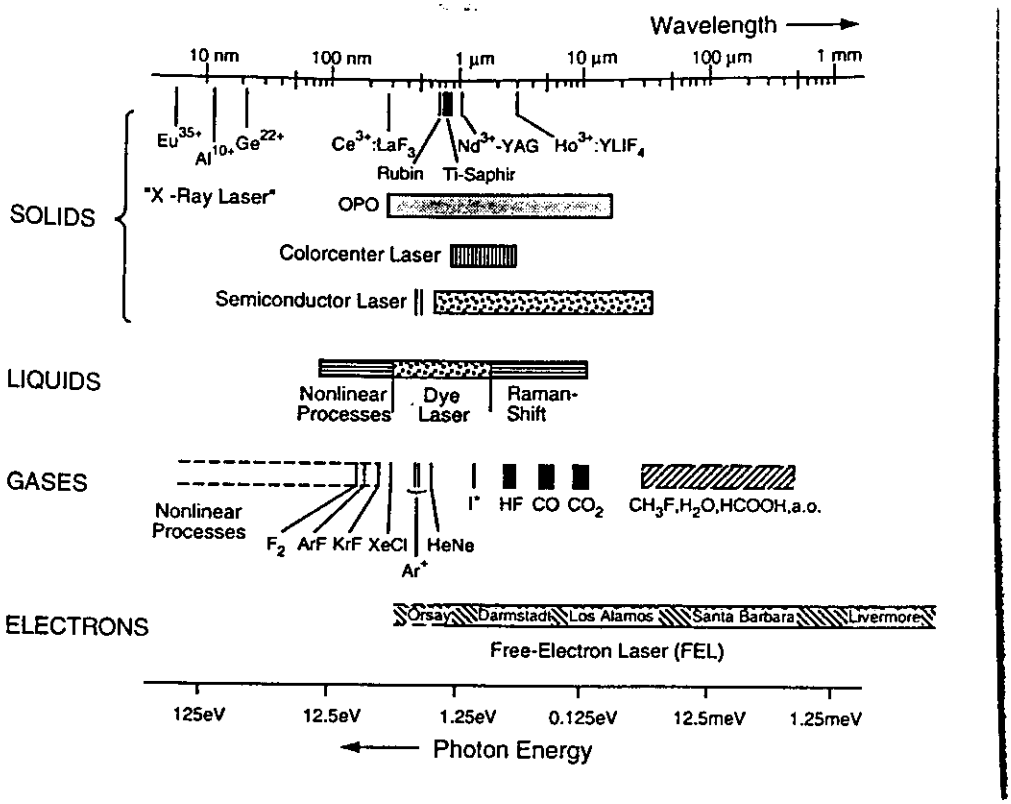

Fig. 1. Wavelength range of Laser light sources

tion of coherent radiation from the far-infrared to the X-ray region. Particularly the introduction of tunable lasers and the development of non-linear optical techniques (already theoretically described in 1931 by Maria Göppert-Mayer [9]) greatly expanded the possibilities of combustion spectroscopy using conventional light sources [10]. Even though higher order polarizations responsible for nonlinear optical phenomena are usually small, signal intensities in higher order wave mixing processes can be large, due to their strong dependence on laser intensities, concentration and interaction length. Nonlinear susceptibilities are enhanced whenever one or more of the frequencies of the interacting laser beams are close to quantum mechanically allowed one- or multi-photon transitions. In microscopic terms the induced oscillating nonlinear polarization arises from the nonlinear mixing of the input waves to produce the same or new frequencies at various sum- and difference frequency combinations of the input frequencies. The spatial resolution of these techniques is determined by the intersection volume of the interacting beams. Another common feature is that all techniques need line-of-sight access to the combustion event, although large window openings as it is necessary often for incoherent methods are not required. The direction of the emitted coherent signal beam is determined by the phase matching condition for efficient signal generation. The various linear and nonlinear coherent methods which have most successfully been used so far in combustion analysis are depicted in Fig. 2. Now the spectroscopic states of atoms and molecules in combustion process can be observed non-intrusively with high temporal, spectral and spatial resolution. The advantages of laser spectroscopic techniques for in-situ diagnostics of unstable species are obvious, but also for stable species more reliable results are obtained compared to probe sampling [11]. The area has been reviewed in several earlier International Combustion Symposium volumes [12-14] and elsewhere [15-21]. Two excellent books by Eckbreth[22] and Demtröder [23] are very helpful for anyone in this field.

Since laser spectroscopic techniques are now a normal working tool in combustion laboratories around the world , a thorough review of the present status is clearly beyond the scope of this brief presentation. Therefore a number of representative examples, arranged in an increasing order of complexity ranging from the dynamics of elementary combustion reactions to the incineration of municipal waste, are selected for discussion in the following pages. However, the examples are drawn heavily from material with which the author has a first-hand experience.

Energy Level Diagram **Beam Geometry** **Signal**

A) ABSORPTION SPECTROSCOPY (ABS)

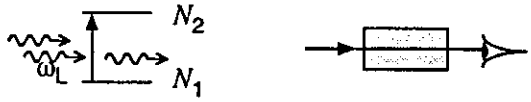

$$I_{abs}(\nu_{12},x) = I_L(\nu_{12},0)\exp[-k_{12}\cdot x]$$

$$\Delta I_{abs} = I_L(\nu_{12},0)A_{12}\frac{N_1 c^2 l}{8\pi\nu^2};\quad N_1 = Nf_B$$

B) LASER INDUCED FLUORESCENCE (LIF)

$$I_{LIF}(\Delta\nu) = \frac{h\nu}{c}\varepsilon\frac{\Omega}{4\pi}A\cdot l\,N_1 B_{12}\frac{\tau_{eff}}{\tau_{rad}}I_L(\nu_{12})$$

C) RAYLEIGH SCATTERING (RS)

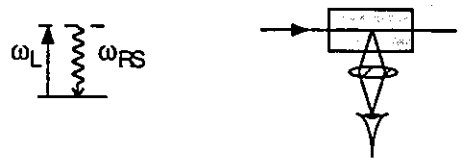

$$I_{RS} = \left(\frac{\partial\sigma}{\partial\Omega}\right)_{mix} I_L N\varepsilon;\qquad \left(\frac{\partial\sigma}{\partial\Omega}\right)_{mix} = \sum_i x_i\left(\frac{\partial\sigma}{\partial\Omega}\right)_i$$

$$\left(\frac{\partial\sigma}{\partial\Omega}\right)_i = \frac{4\pi^2(n_i-1)^2\nu_L^4}{N^2c^4}$$

D) SPONTANEOUS RAMAN SCATTERING (SRS)

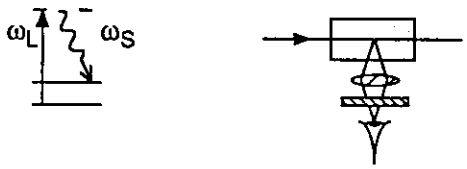

$$(I_{SRS})_{zz} = N\left(\frac{\partial\sigma}{\partial\Omega}\right)_{zz} I_L\cdot\varepsilon$$

$$\left(\frac{\partial\sigma}{\partial\Omega}\right)_{zz} = \frac{h(\nu_L-\nu_{12})^4}{8mc^4[1-\exp(hc\omega_e/kT)]}\left\{(a')^2+\frac{4}{45}(\gamma')^2\right\}$$

E) COHERENT ANTI-STOKES RAMAN SCATTERING (CARS), $\omega_{CARS} = 2\omega_1 - \omega_2$

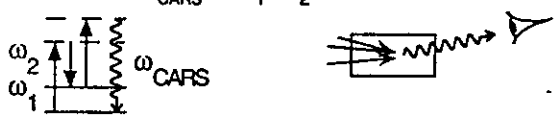

$$I_{CARS} = \frac{\omega_3^2}{n_1^2 n_2 n_3 c^4\varepsilon_0^2}l^2 I_1^2 I_2\left|\chi_{CARS}\right|^2$$

$$\chi_{CARS} = \left(\frac{N\Delta_j c^4}{\hbar\omega_2^4}\right)\cdot\left(\frac{\partial\sigma}{\partial\Omega}\right)\cdot\frac{1}{\Gamma_j}+\chi_{nr}$$

F) DEGENERATE FOUR WAVE MIXING (DFWM), $\omega_{DFWM} = 2\omega_1 - \omega_1$

$$I_{DFWM} = k_{12}^2 l^2\frac{4(I/I_{sat,0})^2}{(1+4I^2/I_{sat,0}^2)^3}I_{pr}$$

$$k_{12} = \frac{\mu^2 N\Delta_{12}kT_2}{2\varepsilon_0\hbar};\qquad I_{sat,0} = \frac{\hbar^2 c\,\varepsilon_0}{2\mu^2 T_1 T_2}$$

G) POLARIZATION SPECTROSCOPY (PS), $\omega_{PS} = 2\omega_1 - \omega_1$

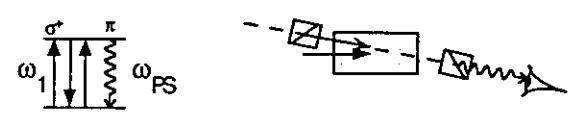

$$I_{PS} \approx I_0\left[\xi+\theta^2+\frac{1}{2}\theta\Delta_{k12}lI_1 S\right];\quad S\equiv\frac{\hbar\omega_1}{\rho\sigma_{JJ'}}$$

H) SUM FREQUENCY GENERATION (SFG), $\omega_{SFG} = \omega_{vis} + \omega_{IR}$

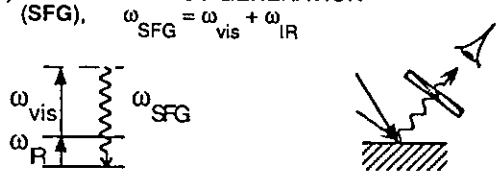

$$I_{SFG} = \frac{\omega_{SF}128\pi^3}{\hbar c^3}\left|L_i K_j^{vis} K_k^{IR}\right|^2\left|\chi_{SFG}\right|^2\frac{I_{vis}\,I_{IR}}{AT}$$

$$\chi_{SFG} = \frac{A_k M_{ij} N\Delta_j}{i\hbar\Gamma_j}+\chi_{nr}$$

I) RESONANCE ENHANCED MULTIPHOTON IONIZATION (REMPI), $n\cdot\omega_1 + m\cdot\omega_2 > \omega_{ion}$

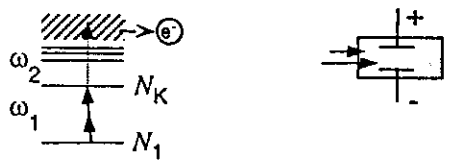

$$S_{REMPI} = N_1\left(\frac{\sigma_{1k}n_{L1}^2}{1+A_k/\sigma_{kl}n_{L2}}\right)$$

Fig. 2

Fig. 2

Survey of linear and nonlinear laser spectroscopic techniques applied in combustion diagnostics. On the left the relevant energy level diagrams are given. Upward facing arrows indicate photon absorption (or conversion); downward facing arrows depict photon emission; $\omega_i = 2\pi\nu$ are the frequencies of the fields involved. The middle column depicts a simplified experimental setup for each method with corresponding beam and detection arrangements. The right column shows approximate analytic expressions for the signal intensity.

A) **Absorption** [24]

$I_L(\nu_{12},0)$: incoming laser intensity; ΔI_{abs}: fractional absorbed intensity for small absorbance; k_{12}: absorption coefficient at frequency ν_{12}, A_{12} Einstein coefficient for spontaneous emission, f_B denotes the Boltzmann fraction and N_1 the population of absorbers in the lower quantum state at temperature T.

B) **LIF** [22]

The LIF intensity is detected over the whole emission bandwidth $\Delta\nu$; τ_{eff} is the effective lifetime of the upper level population, which is reduced by, e.g., spontaneous emission, collisional electronic quenching, vibrational and rotational energy transfer, predissociation, ionization and chemical reaction. B_{12} is the Einstein coefficient for stimulated absorption, τ_{rad} the radiative lifetime of the upper level. Ω denotes the collection solid angle and ε the collection efficiency from a cylindrical probe volume of cross section A and length l.

C) **RS** [22]

I_{RS} is the Rayleigh intensity scattered into a solid angle Ω at 90 degrees from the incident laser beam, $(\partial\sigma/\partial\Omega)_{mix}$ the differential Rayleigh cross section for excitation in a mixture of different species i at a total number density N of scatterers in the probe volume and $(\partial\sigma/\partial\Omega)_i$ the Rayleigh scattering cross section for species i, with mole fraction x_i and refractive index n_i.

D) **SRS** [22,25]

$(I_{SRS})_{zz}$ is the Raman radiant intensity scattered into a solid angle Ω at 90 degrees from the incident laser beam, $(\partial\sigma/\partial\Omega)_{zz}$ the differential Raman cross section (vibrational-rotational scattering) for excitation and detection with parallel polarization for a rotationally unresolved vibrational line, N the number of scatterers in the probed volume, ν_{12} the Raman transition frequency. The term in curly brackets is equal to the square of the derived and spatially averaged induced polarizability, with the average polarizability a and the polarizability anisotropy γ . $1/[1-\exp(hc\omega_e/kT)]$ is the summation over all populated vibrational levels at temperature T for a harmonic oscillator.

E) **CARS** [22,25, 26]

The CARS signal intensity is radiated at frequency $\omega_3 = 2\omega_1 - \omega_2$. l is the interaction length of the overlapping beams; χ_{nr} the nonresonant (real) susceptibility of the medium, Γ_j the Raman line width in cm^{-1} of the probed transition. The third order nonlinear susceptibility $\chi^{(3)}$ of the medium is derived for an isolated Raman transition (off electronic resonance) [25]. Δ_j is the population difference the upper and lower Raman levels and between ω_2 is the Stokes frequency.

F) **DFWM** [22, 27, 28]

The expression is valid in the limit of low absorption ($k_{12}l << 1$), saturating pump beams and weak probe and signal beams; T_2 is the coherence dephasing time, μ_i the transition dipole moment, $I_{sat,0}$ the saturation intensity at line center and T_1 the population relaxation time.

G) **PS** [22, 29]

The signal intensity expression is valid for a linearly polarized pump beam oriented at 45 ° to the probe polarization. Δk_{12} is the maximum linear dichroism ($k_z - k_x$). I_0 is the probe intensity ξ the extinction coefficient of the polarizers, θ the polarizer uncrossing angle, S the saturation parameter for a pulse of length t, and $\sigma_{JJ'}$ are the Clebsch-Gordan coefficients.

H) **SFG** [30,31]

The signal intensity is in photons per pulse; χ_{SFG} is the second-order nonlinear optical susceptibility of the surface adsorbates; L_i, $K_{j,k}$ are the Fresnel factors, A the beam area overlapp on the surface and T the pulse duration of the infrared (IR) and visible (vis) laser beams. A_k, M_{ij} are the dipole matrix elements for infrared and Raman active transitions, respectively.

I) **REMPI** [23]

The signal rate S_{REMPI} (counts/s) is determined by N_1: density of molecules in the ground state, σ_{1K}: absorption cross section for transition $1 \rightarrow k$; n_{L1}: number of incident laser photons; A_k: transition probability for multiphoton transition $1 \rightarrow k$; n_{L2}: number of photons/pulse for ionization laser; σ_{kI}: ionization cross section.

Dynamics of Elementary Gas-Phase Combustion Reactions

Despite the large number of elementary chemical reactions taking place during the oxidation of hydrocarbons, important parameters of combustion processes are often controlled by few elementary reactions. As shown by Warnatz [32] with respect to the calculated flame velocity of a stochiometric propane-air flame, the product of sensitivity and uncertainty is especially high for the following two simple elementary reactions

$$H + O_2 \rightarrow O + OH \qquad (1)$$

$$HO + CO \rightarrow CO_2 + H \qquad (2)$$

which should therefore be characterized in great detail and with high accuracy. The final goal is to have for such elementary steps a consistent picture of the results of quasiclassical trajectory (QCT) and quantum mechanical scattering (QMS) calculations on accurate ab initio potential energy surfaces (PESs) with experimental data from reaction dynamics and kinetic investigations. The dynamics of tri- and tetraatomic elementary gas-phase reactions can be studied in microscopic detail by combining short pulse laser photolysis (LP) to generate translationally excited reactants with a time-, state- and orientation-resolved product detection by laser induced fluorescence spectroscopy (LIF). As illustrated in Fig. 2, LIF uses a tunable laser which is scanned through an absorption band of a molecule or over the absorption line of an atom. Once a transition between specific internal energy levels is excited, the resulting total fluorescence (excitation spectrum) or the spectrally resolved fluorescence (fluorescence spectrum) is detected.

From relative line intensity measurements species concentrations and internal quantum state distributions can be determined with high sensitivity (e.g. 10^3 particles per OH quantum state, single atoms). Figure 3 shows a schematic description of the application of the LP/LIF "pump-and-probe" method [33] to reaction (1). In such dynamics experiments [34] it was observed that with increasing collision energy the nascent OH product rotational state distribution continuously changes from a statistical to a non-statistical one. This behaviour could be well reproduced by QCT calculations and is attributed to a change of the underlying reaction mechanism from a HO_2 complex forming pathway at lower energies to a direct one at higher collision energies. Beside providing insights into the microscopic reaction dynamics, absolute reaction cross sections (σ) can be measured directly with this laser technique. If the complete dependence of σ on the relative kinetic energy (E) is determined (excitation function) the thermal rate constant k(T) can be obtained.

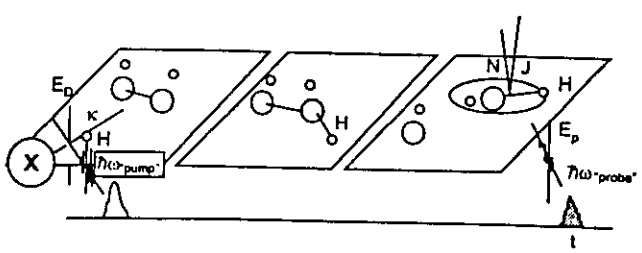

Fig. 3 Schematic describtion of the LP/LIF "pump-and-probe"method

When translationally energetic H atoms are generated by pulsed laser photolysis of HX-type precursor molecules in a large excess of a moderator gas, the initially present nascent nonequilibrium H atom velocity distribution evolves toward the thermal equilibrium distribution determined by the temperature of the moderator gas. When, in addition, a reagent is present, reactive collisions occur in competition with the translational relaxation. In this way the excitation function σ (E) and reaction threshold can be determined. Figure 4 shows a laser arrangement for such measurements for the prototype bimolecular reaction [35]

$$H + D_2 \rightarrow HD + D \qquad (3)$$

in which H and D atoms were detected with sub-Doppler resolution via ($2p\,^2P \leftarrow 1s\,^2S$) laser-induced fluorescence, using narrow-band ($\Delta\nu_{VUV} = 0.4\ cm^{-1}$) VUV laser radiation generated by resonant third-order sum-difference frequency conversion ($\omega_{VUV} = 2\,\omega_R - \omega_T$) of pulsed dye laser radiation (pulse duration ~ 15 ns) in a phase-matched Kr-Ar mixture. The frequency ω_R ($\lambda_R = 212.55$ nm) was resonant with the Kr 4p-5p two-photon transition while ω_T could be tuned from 844 to 848 nm to cover the H/D atom Lyman-α transitions. The Lyman-α light is separated from the unconverted laser radiation by a lens monochromator. Experimental results are depicted in Fig. 5 together with theoretical reaction cross sections. In order to account explicitly for the experimental conditions the theoretical reactive cross sections were averaged over a room-temperature Boltzman distribution of the D_2 rotational states. Both the QCT [36] and the QMS [37] cross sections show excellent agreement with the experimental results [38].

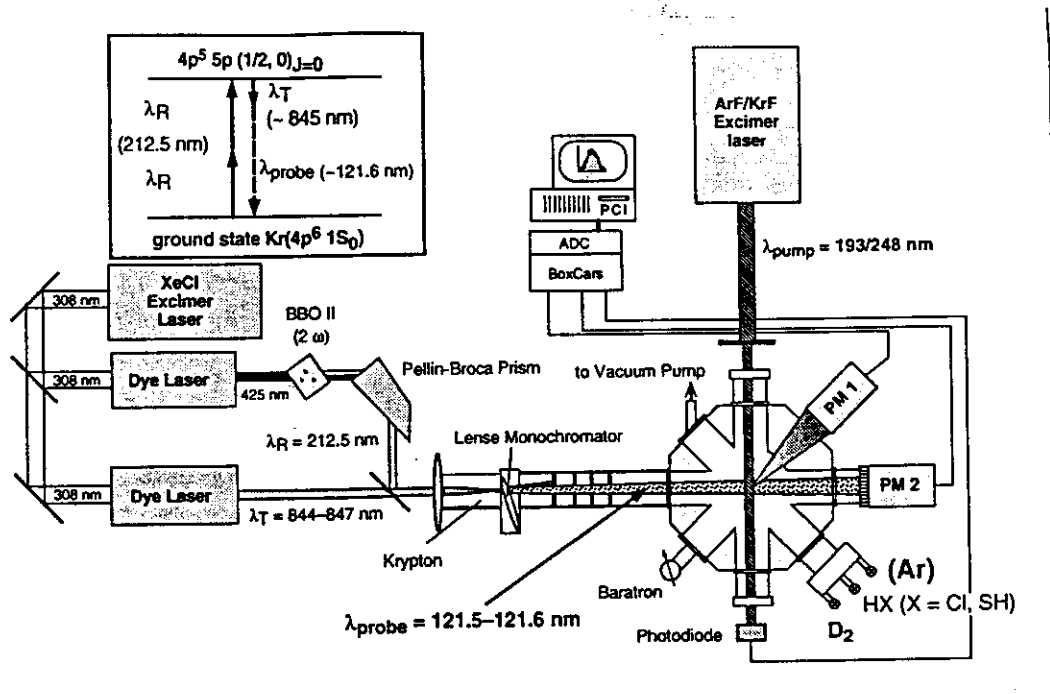

Fig. 4. LP/LIF setup for dynamics studies of the $H + D_2 \rightarrow HD + D$ reaction (3).

However, this is in the case of the classical calculations probably the result of some fortuitous cancellation of two opposing errors. The first is the absence of tunneling which tends to make the QCT cross sections too small, while the second is the absence of vibrationally adiabatic zero-point energy constraints, which tends to make the QCT cross sections high [39]. Similar observations were made by Wrede et. al. [40] in high-resolution scattering studies of reaction (3) and by Miller [41] in the probable fortuitous agreement of QCT calculated thermal rate coefficients with experimental kinetic data [42] for reaction (1).

Figure 6 shows a comparison of absolute reactive cross sections for reaction (1) from laser-based reaction dynamics studies [43] and QCT calculations [44,45]. Calculations carried out by Varandas [46] are also shown: he extrapolated QMS results for total angular momentum equal to zero (J = 0) to higher J-values. Total angular momentum values up to J = 57 had to be included. This, as a consequence, makes rigorous quantum mechanical calculations a formidable task. In addition, up to now all the reactive scattering calculations were carried out on a single-valued $^2A''$ ground-state surface which in C_s geometry correlates directly *via* the ground state of the HO_2 radical to the products $O(^3P)$ and $OH(^2\Pi)$. However, there are several energetically low-lying electronically excited states which correlate with the same products and could therefore be involved in the

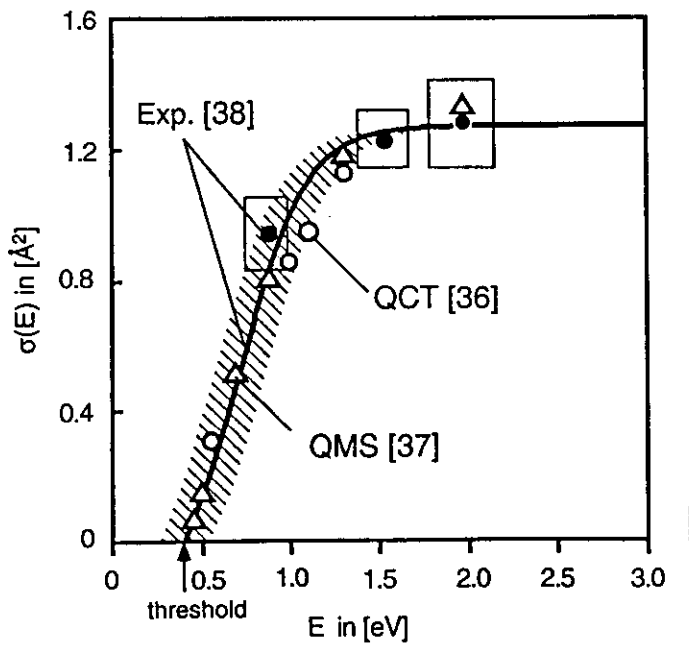

Fig. 5. Absolute reactive cross sections for the reaction $H + D_2 \rightarrow D + HD$ (3).

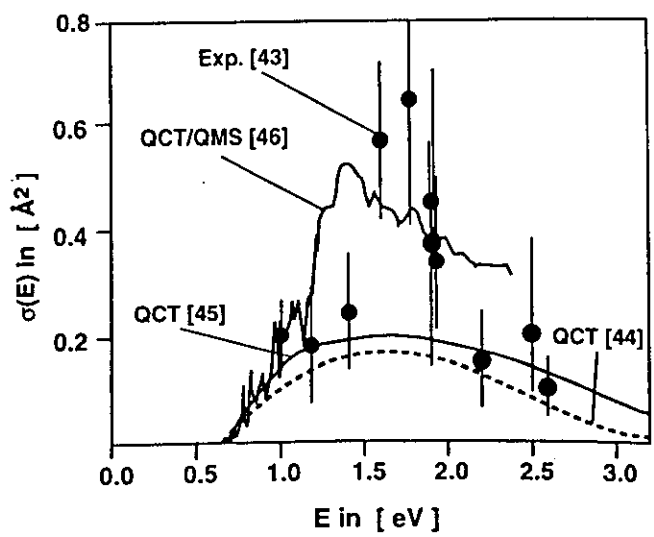

Fig. 6. Absolute reactive cross sections for the reaction $H + O_2 \rightarrow OH + O$ (1).

real reaction process. The true ground-state surface should have two conical intersections, one for C_{2v} and one for $C_{\infty v}$ geometry. In dynamics experiments by Hall and co-workers [47], Doppler-resolved OH LIF was used to determine differential cross sections for reaction (2) at different collision energies. The oberserved energy dependence of the differential cross section was proposed to be a consequence of the dynamics in the vicinity of the C_{2v} conical intersection. Using a DIM (diatomics in molecules) model, a global PES was derived which includes both of the above mentioned conical intersections [48]. Accurate 3D quantum scattering calculations were carried out for thermal collision energies in which geometric phase effects due to the C_{2v} conical intersection were included [49]. In these calculations, significant changes due to the geometric phase effect were observed in the state-to-state transition probabilities.

While the large sensitivity of reaction (1) is caused mainly by its chain-branching character, reaction (2) is dominating due to its large heat release. Absolute reaction cross sections for reaction (2) were measured [50] with the apparatus depicted in Fig. 4. As shown in Fig. 7, the experimental results agree with results of QCT [51], 3D-QMS [52] as well as with quantum-classical(QC) [53] calculations. In real-time measurements carried out by Zewail and coworkers, the lifetime of the $HOCO^{\dagger}$ complex formed in the reaction could be directly determined using laser photolysis of HI inside an $HI\cdots CO_2$ van der Waals complex and monitoring the delay in the appearance of the OH with picosecond time resolution [54]. Experiments with femtosecond resolution were carried out by Wittig and coworkers [55], where a good agreement between the measured OH build-up times and the results of RRKM [56], QCT calculations [57] and reduced dimensionality QMS calculations [58] was found.

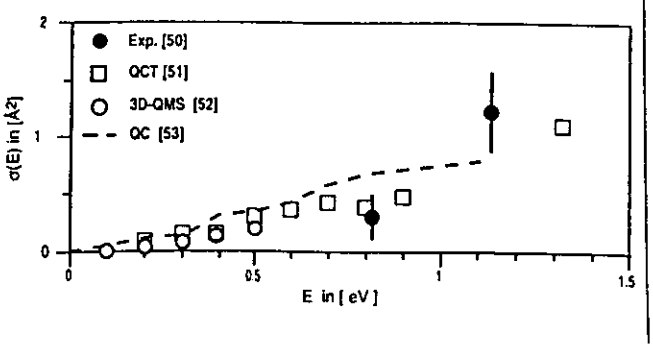

Fig. 7. Absolute reactive cross sections for the reaction $HO + CO \rightarrow H + CO_2$ (2).

Chemical Kinetics

As discussed in the previous section, the gas phase oxidation of CO is not a simple abstraction reaction due to the intermediate formation of the HOCO radical[59,60]:

$$HO+CO \rightarrow HOCO^{\dagger} \rightarrow H+CO_2 \qquad (2')$$
$$\downarrow M$$
$$HOCO+X \rightarrow \text{products}$$

This behaviour causes a complicated temperature and pressure dependence of the thermal rate coefficient k_2 which demands kinetic measurements over a wide temperature and pressure range. Such measurements can be carried out using LIF pump-probe techniques in thermostated flow systems and laser absorption spectroscopy in shock tube experiments. Under the experimental conditions in shock tubes, laser absorption spectroscopy proved to be a key technique to simultaneously measure time histories of the absolute concentrations for multiple product and educt species. The necessary time resolution, sensitivity and species selectivity was achieved through the development of continously tunable, high-resolution laser light sources like ring-dye or diode lasers. Their direct access to strong electronic or rovibrational transitions in the ultraviolet or infrared allowed sensitivities in the ppm range, while the high spectral resolution ensured species selectivity even in complex mixtures. Figure 8 depicts a shock tube setup combining an Ar^+ pumped ring-dye laser and an infrared lead salt diode laser, which were wavelength locked to OH in a flame and to CO_2 in a reference cell to acquire rate coefficients for reaction (2) over the temperature range from 1250 to 1860K (s. Fig. 10) by simultaneous detection of the time histories of products and educts (OH at 306nm, CO_2 at 4.2μm) [61]. If, as for shock tube experiments, a time resolution in the μsec range is necessary, only the peak absorption coefficient is recorded, leading to fractional absorption sensitivities around 1%, using direct detection in the depicted two beam-setup. To convert the measured time histories into absolute species concentration (or mole fraction) via the Lambert-Beer relation (s. Fig. 2), the absorption coefficient $k(\nu_{12})$ has to be calculated. Hence, detailed knowledge is required on the physical and chemical conditions in the post-shock gases, the temperature-, pressure- and species-dependent line broadening mechanisms and the temperature- dependent absorption line strength. As a consequence, this type of experiments can only be applied to spectroscopically well-characterized absorber species

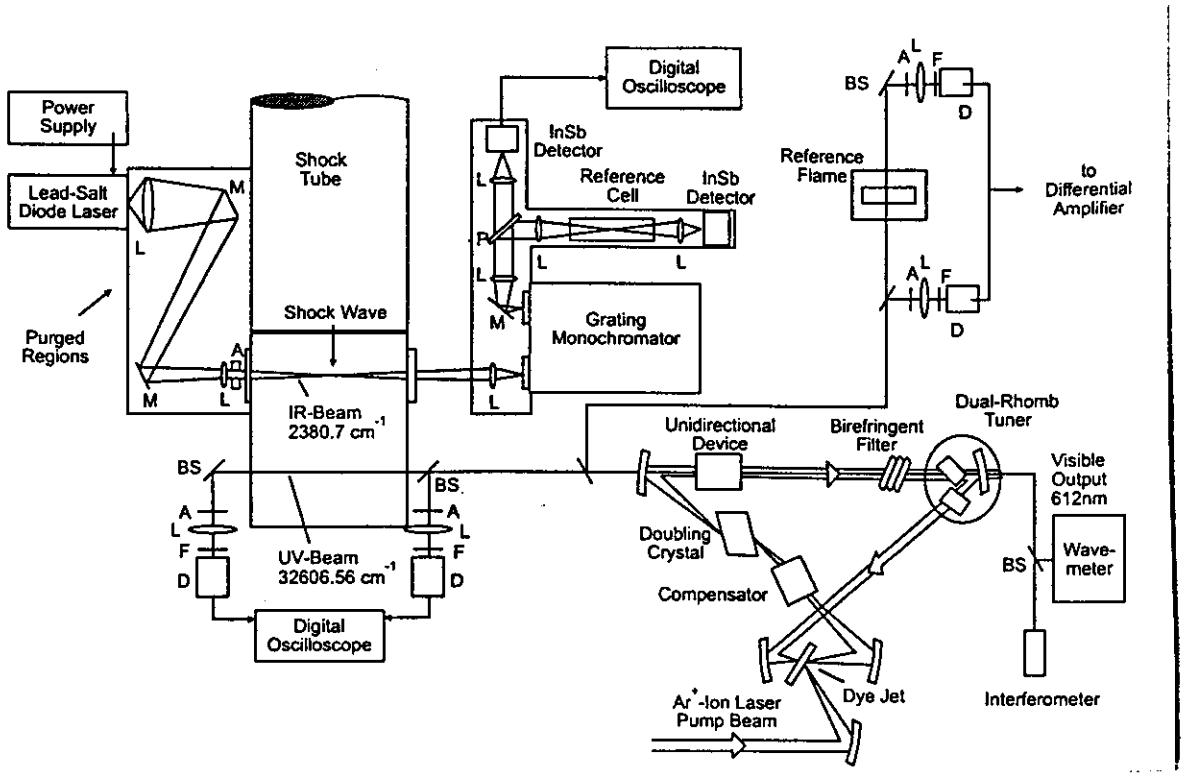

Fig. 8. Shock tube setup for reaction kinetics experiments using high-resolution laser absorption spectroscopy [61,62].

in a well-defined environment. At more moderate time resolution (≈50 µsec), this restriction is lifted to a large extent by rapid tuning dye lasers (up to 4 kHz[62]) or current tunable diode lasers (> 10 kHz [63]) which allow detection of the complete absorption line shape instead of the peak absorption. The information contained in the absorption profile can be used to simplify the interpretation of the concentration signal by spectral integration of the entire absorption profile, thereby removing the signal dependencies on line broadening and, hence, the need for a pressure measurement. Alternatively, if the spectroscopic parameters of the transition are known, the profile of one or multiple lines of the same species can be used to simultaneously infer a multitude of gas dynamic parameters like species concentration (from the area of the line profile), translational temperature (Doppler-width of the profile), pressure (collisional contribution to the total line width), gas velocity (Doppler shift of the line center) and mass flux (measured velocity and concentration). The capability of these techniques is shown in Fig. 9 by infrared diode laser absorption measurements of H_2O in a hypersonic (4500 m/s), high enthalpy (10MJ/kg) shock tunnel [64].

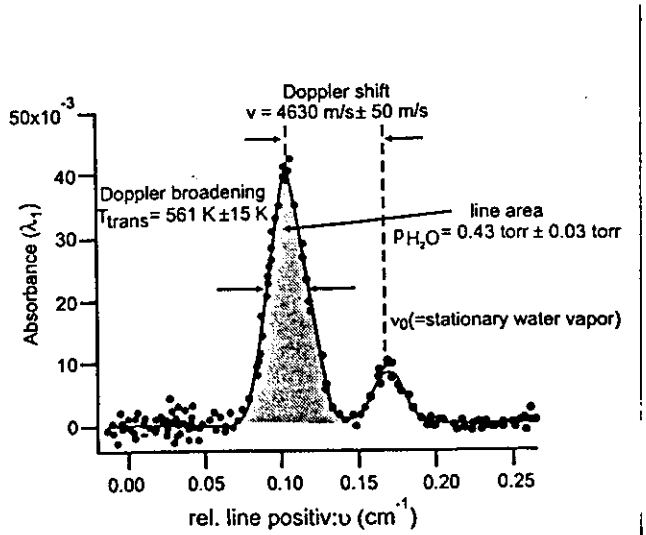

Fig. 9. Infrared diode laser absorption measurements of H_2O in a shock tunnel [64].

Lower temperature rate constants of reaction (2) have been measured by saturated laser-induced fluorescence (SLIF)[65]. This method minimizes the influence of excited-state collisional quenching and is discussed in detail in the section on laminar flames. The experimental data obtained in a wide pressure range [66] are depicted in Fig. 10 together with opitmized E' and J' resolved rigid activated complex RRKM calculations with simplified E and J resolved pressure-dependent collision efficencies [67]. Using LIF spectroscopy also the limiting high pressure rate constant (s. Fig. 10) can directly determined by following the vibrational relaxation of OH radicals in collisions with CO molecules:

$$HO\ (v=1) + CO \rightarrow HO\ (v=0) + CO \qquad (2'')$$

On the other hand monitoring vibrational exci-

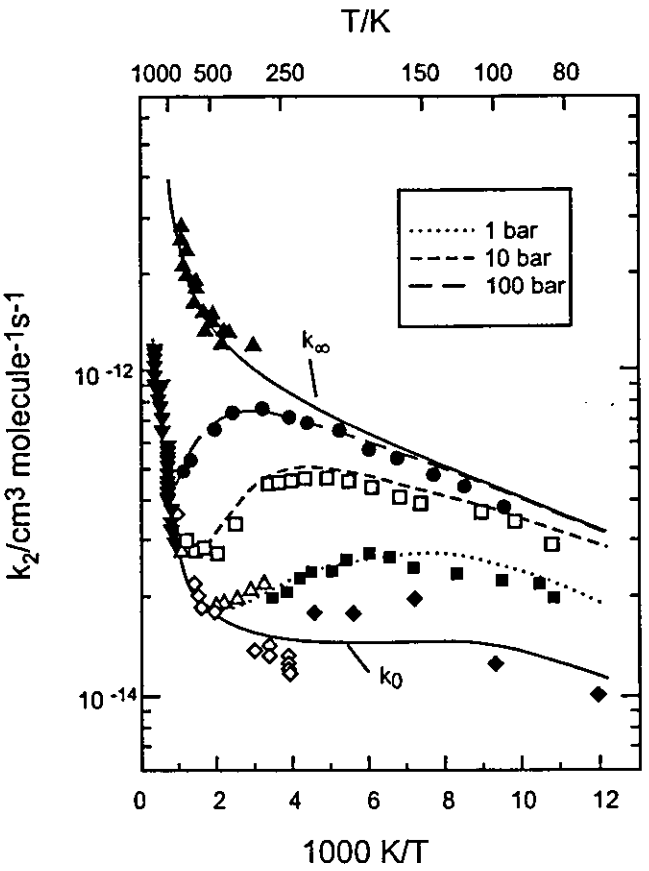

Fig. 10.Temperature and pressure dependence of the rate coefficent k_2 [61, 66, 67].

ted CO with a CO-laser shows a decrease of the rate constant for

$$HO + CO\ (v=1) \rightarrow CO_2 + H \qquad (2''')$$

by a factor of two at room temperature [68]. This observation was also confirmed in shock tube experiments at higher temperatures [61]. Laser detection of CH radicals by absorption [69,70] and SLIF [71]has provided rate data for the initial step in the Fenimore mechanism for prompt NO formation in hydrocarbon flames

$$CH+N_2 \rightarrow CHN_2^{\dagger} \rightarrow HCN + N \qquad (4)$$

$$\downarrow$$

$$CHN_2 + X \rightarrow \text{products}$$

also in a wide temperature and pressure range. The NO formed from the oxidation of HCN can be partially reduced to N_2O, a potent absorber of infrared radiation in the atmosphere, by the reaction with NH or NCO.

$$NO + NCO \rightarrow N_2O + CO \qquad (5)$$

$$\rightarrow N_2 + CO_2$$

In contrast to the reactions (2) and (4), no minimum in the Arrhenius diagram for k_5 in the

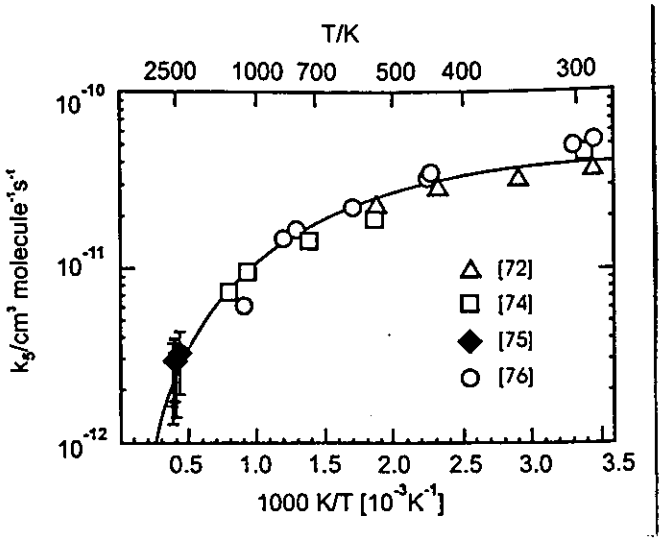

Fig. 11. Temperature dependence of the rate coefficient k_5.

temperature range 298 to 2660 K was identified from direct rate measurements so far (see Fig. 11, [72-76]). The product branching ratio into the N_2O channel increases with temperature [77] and has been measured between 296 and 623 K by combining laser photolysis and time-resolved infrared diode laser species detection [73].

The sensitivity for product and educt detection for laser absorption spectroscopy can be enhanced by using a Herriott-type multiple-pass resonator design. The diameter of the pump laser can be matched to overlap the probe laser in an area which can be heated to give a flat temperature profile. Since the laser is plane-polarized, the number of pathes can be doubled by polarization separation of the counter-propagating

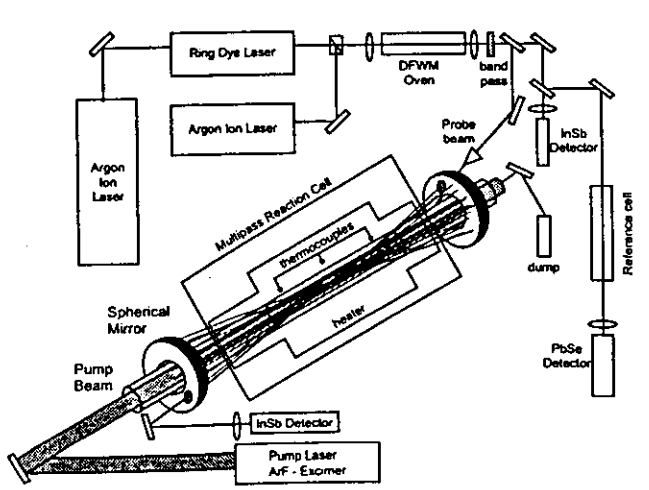

Fig. 12. Laser photolysis/infrared long-path absorption apparatus. The infrared beam from difference frequency mixing of a ring dye laser and an Ar^+ laser is incorporated into a Herriott-type multipass cell.

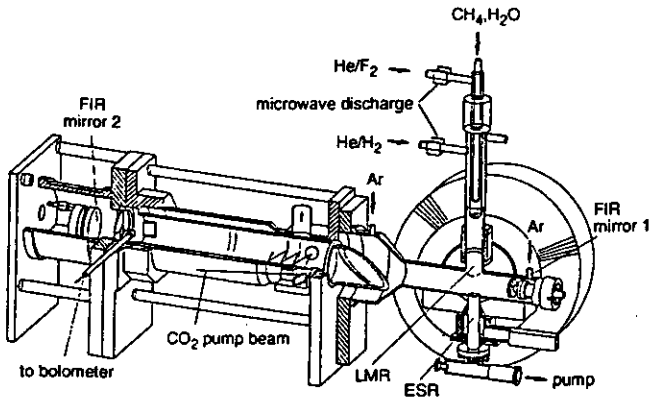

Fig. 13. Combination of a LMR and an ESR spectrometer to detect free radicals and atoms in a low pressure discharge flow system.

beams [78]. Flexible absorption sources are difference frequency mixing processes to generate a continuous wave infrared laser beam [79] and the application of color center or tunable infrared distributed feedback diode lasers [80]. A further enhancement of detection sensitivity can be achieved by placing the absorbing sample within the cavity of a laser. Such intracavity absorption is applied in laser magnetic resonance (LMR) spectroscopy of free radicals. Here, lines of absorbers with high dipole moments are frequency-shifted via magnetic or electric fields until they match strong lines of fixed frequency lasers in the near or far infrared (s. Fig. 1). A large number of laser lines in the far infrared is obtained by vibrational excitation of suitable molecules such as CH_3OH with a CO_2 laser. Absorption is measured by monitoring the change in laser intensity as function of the strength of the external magnetic or electric field. For sensitivity improvement, the field is modulated during scanning so that one obtains first derivatives of the spectra. The high sensitivity of 10^6-10^{10} particles per cm^3 allows detection of free radicals in small concentrations (s. Fig. 13). Such arrangements have been used first to measure the rates of reaction (6) [81:

$$NO + HO_2 \rightarrow NO_2 + OH \qquad (6)$$

More recently important reaction systems such as

$$CH_3 + OH \leftrightarrow CH_3OH^{\dagger} \leftrightarrow {}^1CH_2 + H_2O \qquad (7)$$
$$\downarrow M$$
$$CH_3OH$$

could be studied giving information on the forward and reverse rate data and therefore also on the value for the heat of formation of the CH_2 radical [82,83].

Heterogeneous CO Oxidation

Since Johann Wolfgang Döbereiner in 1823 used platinum (Pt) to ignite a H_2-air mixture at room temperature in his laboratory in Jena, heterogeneous combustion has attracted many investigators. However, compared to gas-phase combustion, the situation is much more complex, since besides the dynamics of the transport processes in the boundary layer above the catalytic surface, also the effects of the topology of the active surface on reactivity, including adsorption and desorption processes, have to be considered. Desorption of OH produced in the oxidation of H_2 on a Pt catalyst, for example, can be studied using the LIF method [84,85].

While in the gas-phase CO is mainly oxidized by OH radicals, on a Pt catalyst direct oxidation by O_2 is possible [86]. As shown in Fig. 14, CO oxidation on Pt proceeds through dissociative adsorption of oxygen reacting in a Langmuir-Hinshelwood reaction with chemisorbed CO [87]. While CO tends to form

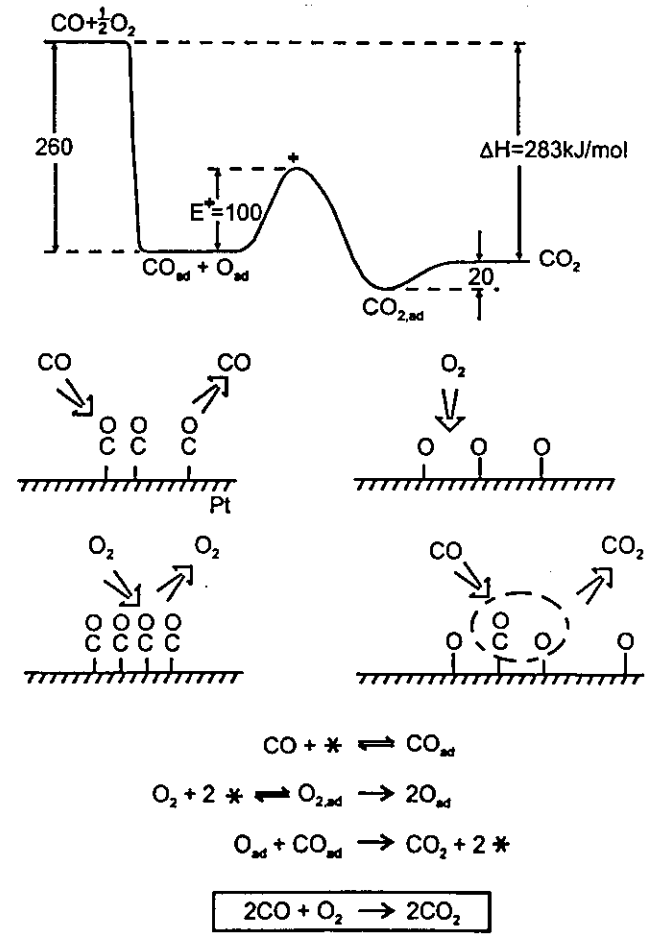

Fig. 14. The Langmuir-Hinshelwood mechanism for the CO oxidation on Pt [87].

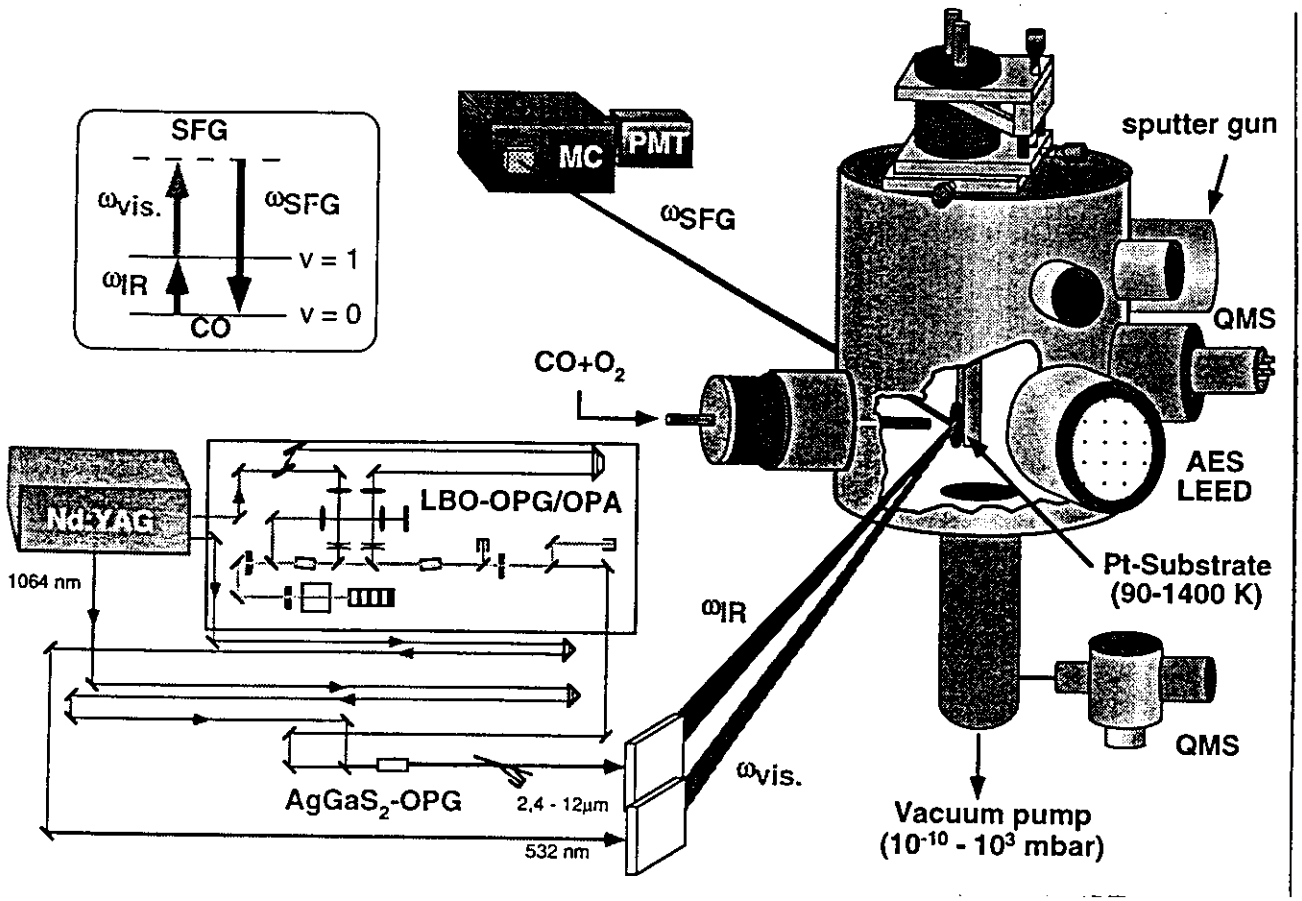

Fig. 15. Experimental setup for the in situ detection of chemisorbed CO during CO oxdiation on Pt.

densely formed adlayers which inhibit dissociative oxygen adsorption beyond a critical coverage, chemisorbed O atoms on the other hand form rather open adlayer phases in which CO may still adsorb. Most of the exothermicity of the reaction is released to the heat bath of the solid during chemisorption of the reactants, while recombination is associated with a fairly small activation barrier and the CO_2 formed is instantaneously released to the gas phase. Studies of elementary surface reaction steps have been carried out mainly under ultrahigh vacuum conditions with well defined single crystal surfaces [88].

Quantitative laser based in-situ diagnostic tools can now be used for the investigation of heterogeneous combustion processes under atmospheric pressure conditions [89]. An experimental arrangement to study the heterogeneous oxidation of CO on a Pt catalyst in a stagnation-point flow geometry by infrared visible sum frequency generation (SFG) is shown in Fig. 15. SFG is a second-order nonlinear optical process (s. Fig. 2) in which a tunable infrared laser beam is mixed with a visible laser beam to generate a sum frequency signal [31]. This process is allowed only in the electric dipole approximation in a medium without centrosymmetry. Therefore, in the

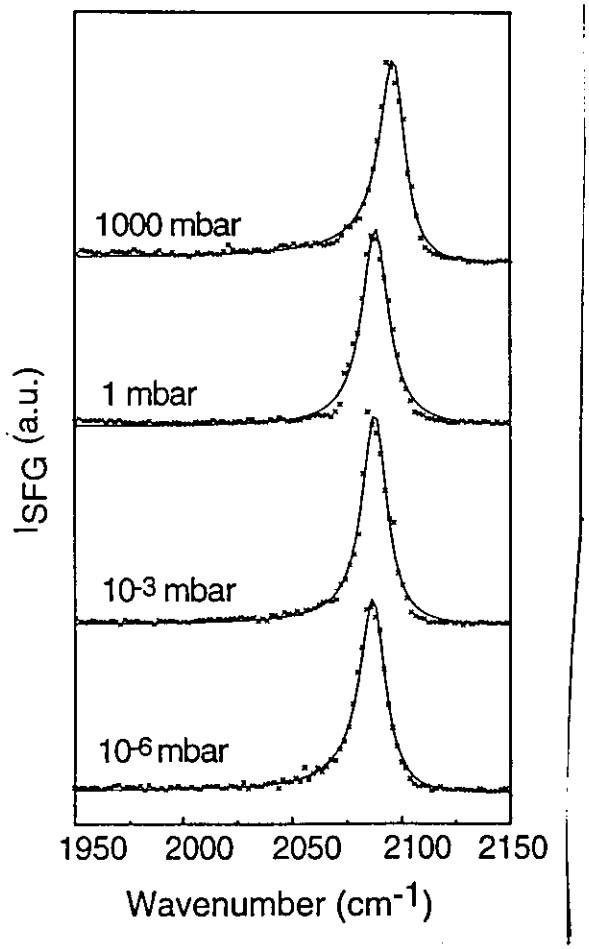

Fig. 16. SFG spectra of CO adsorbed on Pt.

gas/surface system, the signal is dominated by a contribution from the surface, where inversion symmetry is necessarily broken. By modeling SFG spectra it is possible to deduce the relative CO surface coverage. In order to do this, the nonlinear susceptibility has to be divided into a resonant part originating from the CO vibration (ω_{CO}) and an non-resonant part, due to electronic excitations of the Pt surface-adsorbate system:

$$\chi_S^{(2)} = \chi_R^{(2)} + \chi_{NR}^{(2)} = \frac{A_R}{(\omega_{IR} - \omega_{CO} + i\Gamma)} + A_{NR}\, e^{i\Phi},$$

Γ is the homogeneous Lorentzian half-width of the CO vibrational mode, and Φ the phase relative to the incoming electric fields. A_R is proportional to the CO coverage. In Fig. 16 SFG spectra of CO adsorbed on a Pt surface recorded in CO oxidation studies in the pressure range 10^{-6}–10^{3} mbar are shown. The Pt substrate temperature was 297 K. Gas flows were 2 sccm of O_2, 2 sccm of CO and 396 sccm of N_2. The SFG signal is plotted versus the frequency of the tunable IR laser. Solid lines represent the results of least-squares fits using the equation described above. Measurements were carried out on a Pt(111) substrate which was cleaned and prepared in the UHV (10^{-10} mbar) by Ar^+ sputtering to produce a realistic catalyst surface with defined defect-site concentrations.

As shown in Fig. 17, when 1 mbar of CO is present in the gas phase, CO coverage remains constant up to 600 K with a slight frequency shift which can be explained by an increasing mobility of the adsorbed CO molecules. In order to explain the significant shift in CO frequency from (2087 ± 4) cm^{-1} to (2035 ± 5) cm^{-1} coupled with the reduction of the CO coverage due to desorption the topology of the surface has to be taken into account. The CO resonance frequency determined from the SFG spectra can be correlated to the type of adsorption site by the empirical relationship between CO stretching vibration ω_{CO} and the coordination number n of the platinum atom on which the CO molecule is adsorbed [90]: ω_{CO} = 1997 + 10 n (cm^{-1}). At low temperature (300 K), the center-frequency is dominated by the CO linear bound at Pt terrace sites (see Fig. 18). With increasing temperature, desorption starts with the weakest bound CO on the terrace sites, followed by subsequent desorption of CO more strongly bound on defect sites (steps, kinks, islands) of the disordered Pt(111) substrate.

In contrast, as soon as oxygen is added at 300 K, the CO frequency shifts to a slightly higher values indicating that depopulation of the defect sites starts first (see Fig. 18). At higher temperatures, the CO coverage decreases significantly while the frequency remains nearly constant at a value typical for CO adsorbed at terrace sites.

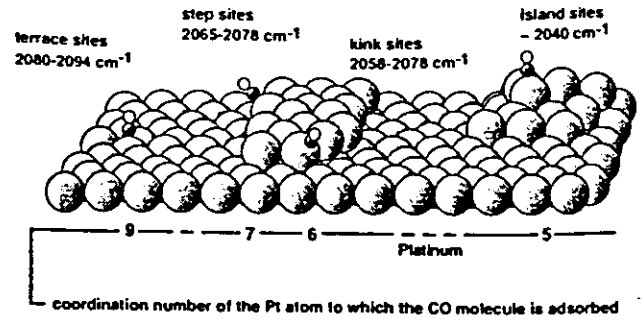

Fig. 18. CO adsorption sites on Pt and the corresponding coordination number of the Pt atom.

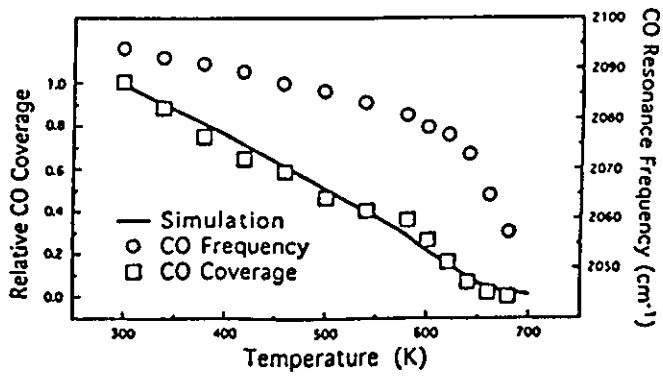

Fig. 17. Temperature dependence of the CO coverage and resonance frequency during CO adsorption / desorption on Pt.

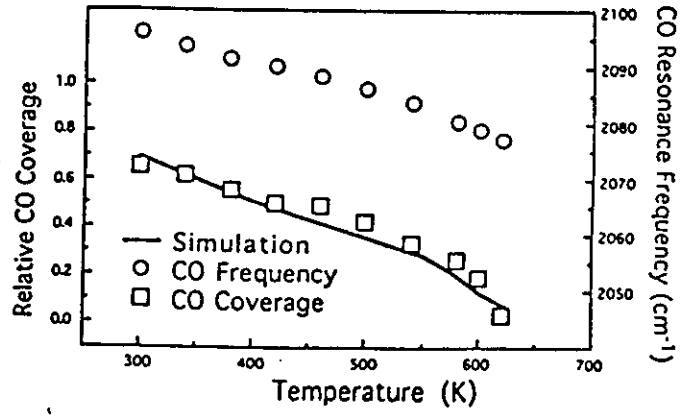

Fig. 19. Temperature dependence of the CO coverage and resonance frequency during CO oxidation on Pt at 20 mbar (Gas flows were 30 sccm of O_2, 15 sccm of CO and 105 sccm of Ar).

This indicates that the reaction takes place predominately at the defect sites. At these free sites further O_2 adsorption followed by reaction with terrace-site CO can occur.

A mean field model using an adsorption energy of 133 kJ/mol and a preexponential factor of 2.88×10^{15} s^{-1} describes the decrease of the CO coverage due to desorption quite well (solid line in Fig. 17). On the other hand, as it can be seen in Fig. 19, the same mean field approach using the surface reaction kinetics data of Ref. [91] cannot reproduce the experimental CO oxidation results. In order to accurately describe the change in coverage during CO oxidation the topology of the surface will have to be included in further Monte Carlo simulations [92]. In addition, effects of structural change in the surface and oscillations in the coverage will have to be investigated.

Laminar Flames

Low pressure flames

Laminar premixed flames at low pressure on a flat-flame-burner constitute an ideal experimental arrangement for studing the interaction of elementary chemical combustion reactions, as first described by the Warnatz mechanism for hydrocarbon flames [93]. Experimental data on temperature as well as on concentration profiles for stable and unstable species are used to validate and further develop mathematical models which predict these profiles by numerical solution of the underlying conservation equations, including convection and molecular transport processes.

Fig. 20 shows such an arrangement used for a low pressure $CH_4/O_2/NO$ flame. Absolute concentration profiles of methyl and hydroxyl radicals as well as nitric oxide are measured by laser absorption spectroscopy. CH and CN radicals are followed by LIF. The quantitative application of LIF in such flames requires information on the dependence of the fluorescence quantum yield on pressure, temperature and chemical composition at the measurement location. In low pressure flames, this can be done by direct measurement of the total fluorescence decay time as a function of the position in the flame with a time resolution in the nanosecond range. To obtain absolute number densities from the LIF signals, the remaining unknown factors (Fig. 2) such as excitation volume and optical collection and transmission efficiency can be determined from the slope of the Rayleigh scattering signal of known amounts of nitrogen in the burner, as described by Luque and Crosley [95]. As shown in Fig. 21 the shape and absolute values of the concentration profiles for OH and CH_3 radicals as well as the initial reduction of nitric oxide are well predicted by the models. However, absolute CN radical concentration [96] are significantly overestimated by all models. More work has to be done on the details of the formation and destruction of CN during the reduction of nitric oxide in the reburn process.

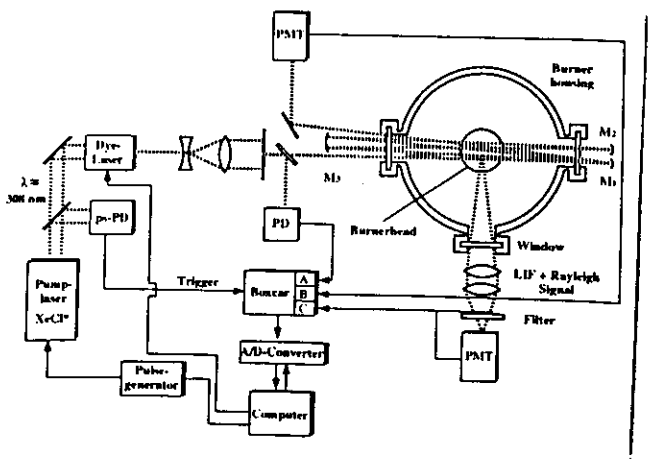

Fig. 20. Experimental setup for laser absorption and LIF spectroscopy in low pressure flames.

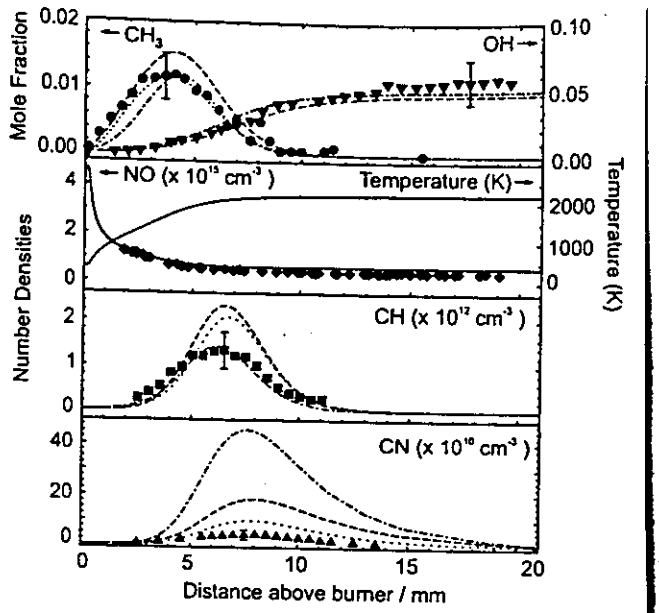

Fig. 21. Comparison of measured and calculated concentration profiles in a laminar $CH_4/O_2/NO$ flame at 10 Torr. Models: (dashed) GRI [94], (dash-dotted) Warnatz [167], (dotted) Lindstedt [96].

Further improvement in sensitive absorption spectroscopy in flames can be obtained by

using the cavity ring-down laser absorption spectroscopy (CRLAS) [97]. This technique circumvents the drawback of the two-dimensional multipass beam arrangements (Fig. 20). In CRLAS, a laser beam is coupled into a linear cavity formed by two concave mirrors with high reflectivity at the species specific wavelength. The trapped light pulse is monitored in time via transmission through the output mirror. The decay time is a quantitative measure of the absorption strength, and hence the concentration of the species. Since only the decay time is relevant, the method also has the advantage of being insensitive to pulse-to-pulse energy fluctuations of the laser source. HCO radicals were detected in low-pressure flames by CRLAS by their weak electronic absorption [98]while CH_4, CH_3, H_2O and CO_2 were monitored quantitatively in a narrow range of their characteristic vibrational transitions in the infrared around 3 μm with high spectral resolution (0.007 cm^{-1}) using an optical parametric oscillator [99].

In recent years, as an interesting alternative to LIF diagnostics in laminar flames and other combustion devices, degenerate four wave mixing (DFWM) has emerged. This one-color variant of the more general resonant four-wave mixing techniques can be visualized as a laser-induced grating (LIG) process [100, 101], in which two beams of equal intensity from one laser are crossed in the probe volume. If the wavelength of these "writing" beams is tuned into resonance with a molecular transition in the sample, then, for parallel, linear electric field polarizations, a population grating (PG) will be formed by absorption in the interference region of both beams. This PG can be "read out" by a third resonant reading beam at the same wavelength with the Bragg condition satisfied for all participating wave vectors. From a simplified expression (s. Fig. 2) for the DFWM intensity generated in an absorbing medium with strong pump- and weak probe- and signal-beams [28, 102] it is obvious that large signal intensities are attainable at higher beam intensities, although saturation effects will make quantitative interpretation of data difficult [103-105]. The dependence of the signal intensity on the absorption coefficient k_{12} makes DFWM a spatially resolved absorption technique for combustion diagnostics which is not dependent on the probed species to fluoresce. This has been exploited to monitor, e.g., species in highly predissociative electronic transitions such as in CH_3 [106]. DFWM spectra have been recorded in laminar flames from OH, NH [107], NO [108], CN [109], NO_2 [110] using electronic transitions. If narrow-bandwidth tunable lasers are employed in the phase-conjugated beam geometry, where both pump beams are counterpropagating, high-resolution scanning DFWM spectra can be obtained [111]. Since the increasing availability of tunable infrared radiation from optical parametric oscillators, the opportunity to monitor hydrocarbons (CH_4, C_2H_2) via their characteristic infrared DFWM spectrum has also been exploited [112].

Another highly selective and sensitive technique for product analysis in laminar flames is resonantly enhanced multiphoton ionization (REMPI) combined with molecular beam sampling mass spectrometry. Detection sensitivities in the lower ppb (10^{-9}) and ppt (10^{-12}) range for chloroethylenes, toluene and p-chlorophenol have been observed [113].

Atmospheric and High Pressure Flames

At higher pressure, collisional effects play an increasing role if quantitative data have to be de-

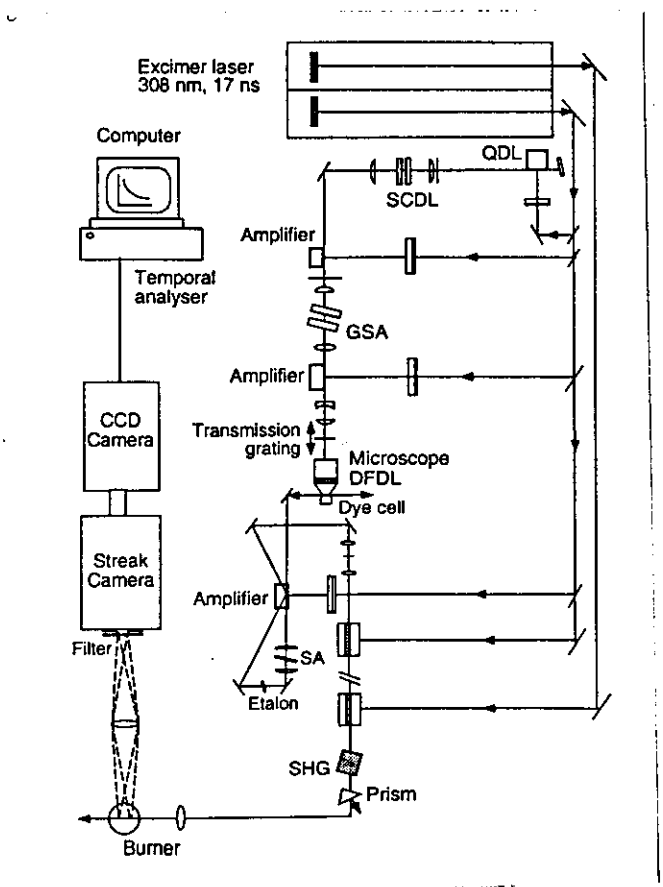

Fig. 22. 1D-measurements of fluorescence lifetimes in an atmospheric pressure flame with a picosecond laser system [113].

rived with laser spectroscopic methods. Using advanced laser equipment, one can investigate these effects directly by shortening the laser pulse length below the collisions times, even at high pressure (PITLIF [114]). Fig. 22 shows a LIF setup with picosecond time resolution. Here, an excimer laser pumps at 308 nm a laser cascade of a Quenched Dye Laser (QDL) followed by a Short-Cavity Dye Laser (SCDL) and a Gated Saturated Absorber (GSA) which shortens the pulsed laser pulse length from 20 ns down to 10 ps. This pulse illuminates a grating which is imaged onto a dye cell using a microscope objective. The beams then produce a Distributed Feedback Dye Laser (DFDL) system with wavelength tunable pulses of 600 fs duration. Fluorescence lifetimes of OH radicals in a premixed laminar burner with a conical flame at atmospheric pressure are measured along a line by imaging a section of the flame into a streak camera [115]. Short pulses allow also collision quenched lifetime measurements with multiphoton excitation of atoms and CO molecules [116].

Using the temperature dependent quenching cross sections as well as rotational (RET) and vibrational energy transfer (VET) rates the time dependent population of relevant quantum states can be described by a rate equation model [20, 21, 117, 118]. Another way to deal with collisional effects is to work at very high laser power densities to saturate the absorption (SLIF). The fluorescence signal then becomes independent of collisional processes and laser power density [65]. However, due to the spectral, temporal and spatial variation of the laser intensity, fully saturated conditions are difficult to achieve in practical experiments. Several strategies have been developed to deal with this problem Mailänder introduced the concept of the saturated volume [119]. Stepowski and Cottereau developed the TOPLIF method in which the saturated fluorescence signals are measured simultaneously in two detection geometries so that corrections for the beam shape effect can be derived from this experiment [120]. For quantitative interpretation of SLIF signals Lucht, Laurendeau and co-workers have introduced the so-called "balanced cross rate model". This model assumes that the net-rates of population transfer in and out of the laser coupled levels are approximately equal [121-123].

Using different laser spectroscopic techniques in combination with mass spectrometric probe sampling spatially resolved profiles of temperature, all major stable species as well as major and minor radical species in a Wolfhard-Parker diffusion flame at atmospheric pressure have been obtained by Smyth and coworkers [124] in order to assess NO production/destruction pathways [125].

At the higher pressures typical of many technical applications, LIF spectra are also affected by line broadening and shifting, which causes changes in excitation efficiency due to varying the spectral overlap of absorption line and laser spectral profile. Furthermore, spectral features of different species may overlap and complicate selective excitation. Spectroscopic studies in laminar high pressure flames can reveal the influence of interfering species and the change of spectra due to line broadening and shifting. As an example Fig. 23 shows excitation-emission spectra of NO in a lean CH_4/air flame between 1 and 40 bar.

A technique which is potentially less susceptible to the quenching phenomena but still shows high sensitivity is polarization spectroscopy (PS) [23]. In PS, a weak linearly polarized probe and a stronger circularly or linearly polarized pump beam are crossed in a nonlinear medium at a small angle. The pump beam creates an anisotropy in the sample by selective absorption within Zeeman sublevels of the involved transition. This causes rotation of the

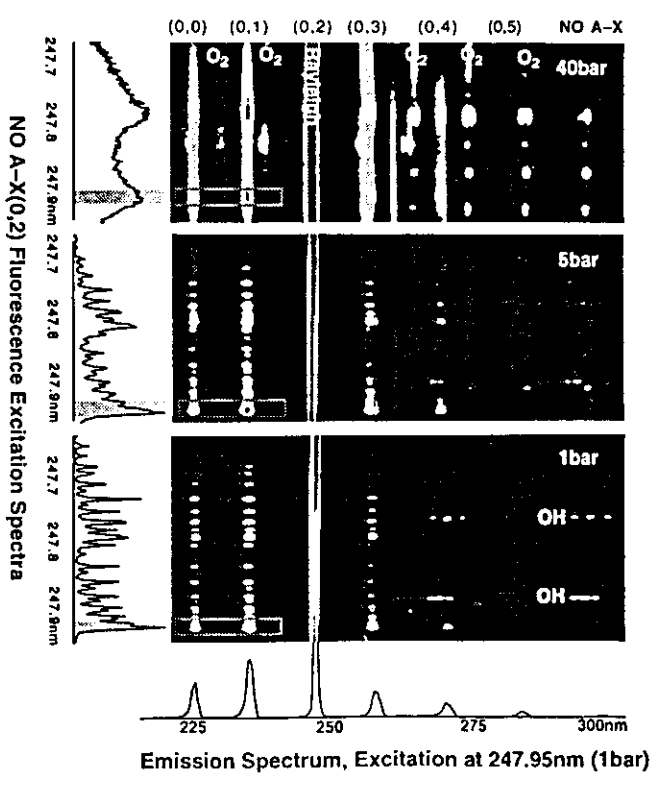

Fig. 23. Excitation-emission spectra obtained in a lean methane/air flame using a tunable KrF excimer laser.

probe beam polarization and depolarization through differential absorption and refraction in the anisotropic sample of left- and right-circularly polarized components of the linearly polarized probe light, which is detected through a crossed polarizer in the probe beam path (Fig. 2). One drawback of PS as a diagnostic for enclosed combustion events are birefringent windows which cause a depolarization of all beams and lead to a hard to control background signal. Zizak et al. [126] were among the first to apply polarization techniques for trace species detection in sodium- seeded flames. For laminar flame diagnostics its potential as a spatially resolved and background-free absorption technique for the detection of minor species such as OH and NO with good sensitivity was demonstrated [127,128]. The potentials of polarization spectroscopy for two-dimensional imaging of these species and single-shot temperature measurements were shown by Nyholm et al. [129]. Careful modeling of electronic transition strengths of OH and NH and laser bandwidth convolutions is essential for accurate in situ temperature measurements in atmospheric pressure flames using PS [130].

Laser spectroscopy also has been exploited for a long time in sooty flames. In these environments the scattered light intensity is affected by absorption of soot precursors at intermediate stages of soot growth of different size, shape and scattering efficiency. The local extinction coefficient is directly proportional to the soot volume fraction [131] and can be expressed quantum mechanically by the Kramers-Heisenberg relationship [23]. From measurements of the fluorescence depolarization ratio, the particle shape can be deduced. In the preheating zone, the absorption spectrum between 200 and 700 nm is determined by the electronic transitions between bonding and nonbonding π-orbitals in hydrocarbons. The size, shape and spatial occurance of soot and its precursors was investigated in detail by D'Alessio and coworkers who were able to interpret absorption / fluorescence spectra recorded in flames of various stoichiometry from a band gap model [132,133]. Soot formation studies in flames burning various fuels have been extended to pressures larger than 100 bar [134].

Extinction measurements are time consuming, are not spatially resolved and preclude the investigation of non-axisymmetric flames. One method with great prospects for obtaining spatially resolved soot volume fractions (along a line of sight or in two dimensions) is laser induced incandescence (LII) [135-138]. In this technique the soot particles are exposed to a high flux of radiation, usually from a fundamental or frequency doubled Nd:YAG laser beam, whose absorption leads to strong heating to temperatures much higher than normal flame temperatures with subsequent partial evaporation. The time-resolved detection of the emitted thermal radiation, after calibration by extinction measurements, constitutes a quantitative measure of the soot volume fraction. Most recently this calibration by a two pulse technique in a two-dimensional sheet: the extinction across the flame is measured by a low intensity pulse before the high intensity pulse is traversing the same spatial region generating LII, which is imaged onto a second camera [139].

Among the coherent Raman processes, CARS is almost exclusively being used in practical combustion diagnostics. This development was initiated through the pioneering work of Taran and coworkers [140] who recorded the first scanning CARS spectra of molecular hydrogen in a premixed natural gas flame. In CARS experiments one fixed frequency (pump) and one broadband (Stokes) laser beam in the visible, with their frequency difference equal to Raman- allowed transitions, are overlapped with a third laser beam (mostly of the same color as the fixed-frequency beam) and focussed into the sample to create, in a four wave mixing process, a fourth beam at the anti-Stokes frequncy, well separated in wavelength from all incoming beams as well as from possible fluorescence and flame luminosity. The CARS radiation then is dispersed in a spectrometer and detected with a CCD camera. The CARS intensity (s. Fig. 2) is dependent on higher powers of both the pump- and Stokes laser intensities as well as on the square of the number density difference between lower and

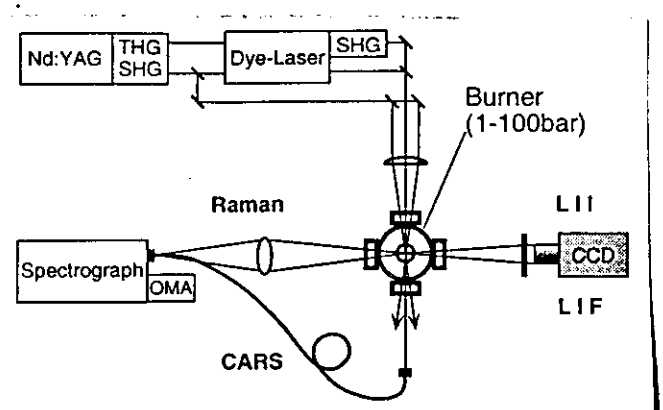

Fig. 24. Experimental arrangement for combined measurements using coherent (CARS) and incoherent (LIF, LII, SRS) laser techniques in high pressure flames.

upper Raman level. The population distribution is contained in the expression of the third-order susceptibility $\chi^{(3)}$ [22]. For low concentrations the (real) nonresonant contribution χ_{nr} is significant and limits the detection sensitivity. The spectral signature of the generated CARS signal is an accurate measure of the gas temperature, which, in well-designed spectrometers can be determined with an accuracy of two percent or better, even in a single laser pulse using advanced fitting codes [141]. High resolution line shape measurements of combustion relevant species such as N_2 [142], O_2 [143], H_2 [144], H_2O, CO[145], CO_2 [146], NO and others have since then improved modeling of CARS spectra as an important condition for precise temperature measurements. Figure 24 exemplifies the most important coherent (CARS) and incoherent (LIF, spontaneous Raman, LII) laser spectroscopic techniques applicable to combustion processes at higher pressures of technical interest. The depicted experimental setup is particularly suitable for a detailled comparison of different techniques applied to the same flame and otherwise identical conditions.

The accuracies obtainable in spontaneous Raman scattering (SRS) and CARS for temperature measurements in high pressure combustion environments is demonstrated in Fig. 25 in a direct comparison between temperature readings as deduced from either spectra of pure rotational Raman or vibrational Q-branch spectra of molecular nitrogen acquired at the same location and under the same operating conditions of a stable high pressure burner. Both measurement sets are well within the 3% limit of precision estimated from the spontaneous Raman data. The latter exhibit well resolved lines even at the highest pressures of 40 bar. In

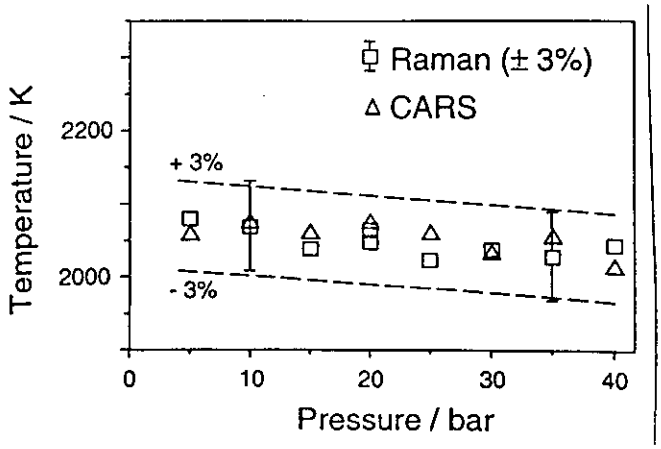

Fig. 25. Comparison of Raman and CARS temperature measurements in high pressure flames.

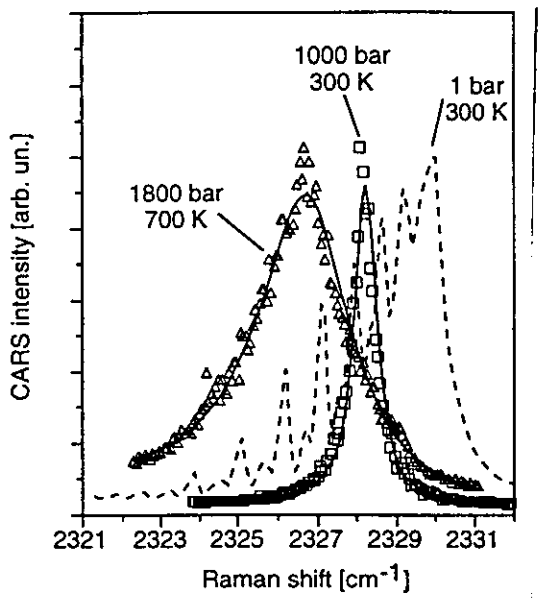

Fig. 26. High-pressure CARS spectra of N_2. Solid lines are the results of a fit using polynomial energy gap (PEG) expression for modeling the state-to-state energy transfer.

contrast, the CARS Q-branch of N_2 shows partial collisional collapse of its rotational structure at the band origin which usually degrades the temperature measurement accuracy at low temperatures (300-700 K). As Fig. 26 shows, this collapse with a corresponding smoothening and narrowing of the whole Q-branch structure is complete in this temperature range and at very high pressures [147-149]. The spectral structure can be modelled satisfactorily using energy gap and scaling laws to predict temperature- and species-dependent rate constants for collision induced rotational energy transfer within the molecule [150, 151].Different models have been employed and tested for nitrogen and oxygen thermometry at higher pressures [147,152]. These studies have provided valuable information about combustion processes under extreme conditions,such as spontaneous ignition, stabilization and burning of diffusion flames in a supercritical mixture of methane and water at pressures up to 2000 bar [153].

Laser Induced Ignition Processes

Optimal control of ignition processes is one of the key factors in improving the performance of many combustion devices. To this end, a better detailed understanding of unsteady combustion phenomena is required. In order to develop

quantitative mathematical models for complete simulation of ignition processes that include detailed chemistry, experimental studies of simple systems are particularly useful. The experimental techniques should allow visualisation of the ignition process in time and space. This can be done by a two-dimensional imaging of OH radicals with planar laser induced fluorescence (PLIF)[154, 155]. The application of tunable excimer lasers with their narrow band width, high pulse energies and high repetition rates allows the effective excitation of short living predissociative states of the OH-radicals (LIPF) [156]. An experimental set-up using this technique to investigate the laser induced ignition process is shown in Fig. 27 [157]. A quartz reactor with suprasil cell walls and SrF_2 windows was used to study the ignition of CH_3OH-O_2-mixtures with a cw CO_2-laser. The coincidence of the 9P12 CO_2-laser line in the (001) - (020) band with the R12-CO stretch fundamental band of the methanol molecule at 9.6 µm allows controlled heating and ignition of the mixture. For temperature measurements, hydroxyl radicals formed during flame propagation can be excited in two rotational states of the (3-0) vibrational band in the $A^2\Sigma^+$-$X^2\Pi$ transition at 248 nm using either two separate KrF-excimer lasers or a single two-wavelength KrF excimer laser [158]. Each excimer laser beam is formed into a light sheet 30 mm in height and 400 µm thick using quartz lenses. The sheets are spatially overlapped with a time delay of 100 ns to separate the signals excited by the different pulses. Reflexion filters consisting of four narrowband dielectric mirrors (297±6nm, transmission >90%, blocking $5x10^4$) were used to isolate the (3-2) fluorescence bands of OH. The fluorescence was detected by gated image-intensified CCD-cameras. The excitation of two different rotational transitions of OH rad icals, starting from N"= 8 and 11, allowed the measurement of spatially corresponding LIF image pairs. Using the Boltzmann distribution, the ratio of these images can be converted into a temperature field (Fig. 28). Calculating temperatures from a two-line LIF measurement requires a careful consideration of a number of effects. The influence of fluorescence quenching, usually the dominating deactivation process for excited OH radicals under atmospheric pressure conditions , is reduced in the experiments by the predissociating nature of the excited state [159,160] to less than 3%. The tunable excimer laser emits polarized light, which in turn induces LIF signals with a spatial preference, depending on the transition that had been excited [161]. Collisions can redistribute the spatial alignment; this means that the ratio of the LIF images can be depend on the nature of the collider gas composition. This effect, as well as the variation of the RET rates in the ground state [162], can be accounted for with a calibration procedure, where temperatures measured by the two-line LIF-method are compared to pointwise CARS temperature measurements [163]. For the direct numerical simulation the two-dimensional system of coupled ordinary differential and algebraic conservation equations was solved numerically by spatial discretization using finite differences [157]. Two-dimensional imaging of the temperature [Fig. 28] as well as the numerical simulation [164] show a conical flame front. This can be explained by the fact that one channel is preheated by the CO_2-laser beam. Therefore the flame propagates faster in the axial than in the radial direction. The fast axial flame propagation is caused mainly by successive ignition along the cell axis, due to different induction times which follow the axial temperature gradient.Typical propagation speeds of the ignited CH_3OH-O_2-mixtures investigated are 30 m/s in the radial direction and 130 m/s in

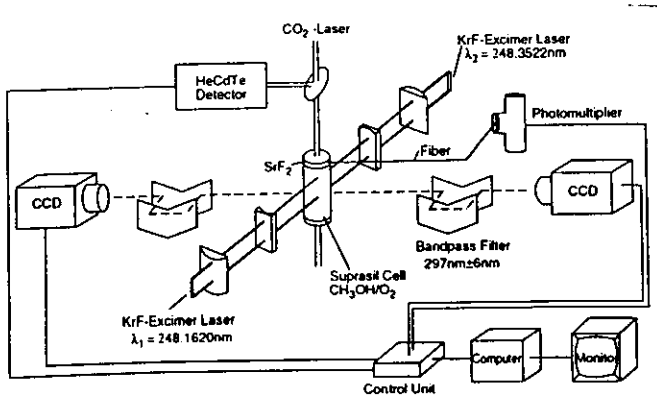

Fig. 27. Experimental setup for studying thermal ignigion processes in CH_3OH/O_2-mixtures [157].

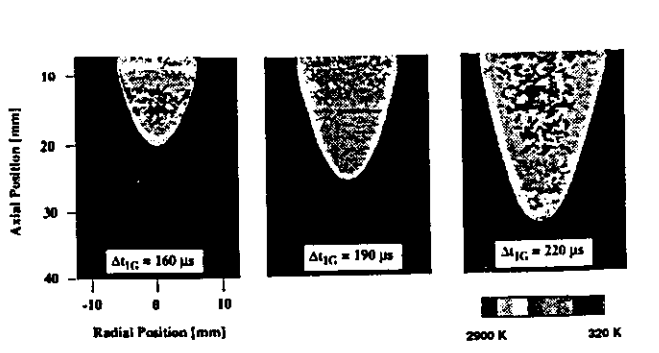

Fig. 28. Development of the temperatue field during CO_2-laser induced ignition of a CH_3OH/O_2-mixture (ϕ = 0.9) [164].

the axial direction. This observation gives an important clue for the understanding of knock phenomena in spark ignition engines. Unwanted self-ignition occurs here due to local temperature fluctuations as small as 20 to 30 K ('hot spots') during the adiabatic compression phase. This local ignition, which can be monitored by PLIF of formaldehyde [165], forms pressure waves which produce temperature jumps, that can accelerate the flame propagation and in the same way as show in Fig. 28. Later on, the combustion wave reaches the pressure wave, and the system is subject to the transition to detonation [166].

Turbulent Flames

Similar to the laminar case, turbulent reactive flows can be described by solving the conservation equations for total and species mass, momentum and enthalpy (Navier-Stokes equations) [167]. However, solving these equations by direct numerical simulation (DNS) is, even in the days of modern parallel computing, a very demanding task. For a realistic system of hydrocarbon oxidation in an internal combustion engine, one would need up to 10^{21} computing steps. In addition, one is generally not interested only in one detailed structure but in averaged and global results for temperature and composition. Therefore at present and for the near future, a direct numerical simulation of three-dimensional turbulent reactive flows in technical combustion systems will not be possible. Instead, turbulence has to be modelled by the use of averaged Navier-Stokes equations, while mean reaction rates can be evaluated with the help of probability density functions (PDF) [167, 168]. To validate such models, multidimensional non-intrusive measurements of species concentrations and temperatures are necessary.

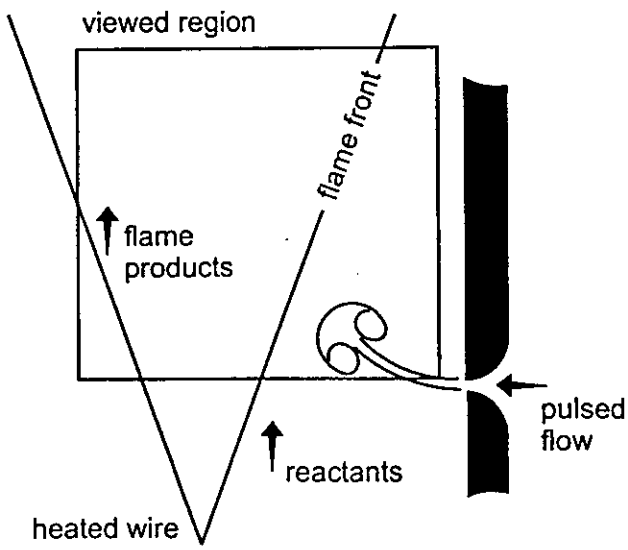

Fig. 29. Schematic of an experimental arrangement to obtain phase-sampled images of vortex-flame interaction by PLIF [169].

Investigations of the interaction of an isolated vortex with a laminar flame provide the basic understanding necessary for modelling turbulence-chemistry interactions, introducing effects of strain, curvature and unsteadiness. Measurement of temporal evolution of the single-vortex flame interaction with a resolution in the kilohertz range is beyond the reach of conventional dye laser systems. However, these measurements are feasible in highly repeatable turbulent systems by phase-sampling of a sequence which then provides the same time-resolved information. Furthermore, phase-locked averaging enables measurements of species with small abundancies and, thus, weak signal intensities. An experiment providing these advantages was set up by Paul et al. [169] using a laminar V-flame and an acoustically driven vortex generator (Fig. 29). The exact position of the flame front, which is identified by the maximum heat release, is of major interest when investigating the turbulence-flame interaction. However, reactive radicals present closly to the flame front, like OH and CH, have given ambigous results in some cases. At high strain rate, the CH front breaks, whereas the OH front persists [169]. From simulation calculations it has been shown that the formyl radical concentration closely matches the distribution of heat release, making it an ideal tracer for the flame front. However, due to the low abundancies and its fast predissociation, LIF-imaging seems to be impossible in unsteady, non-reproducible turbulent sytems. LIF measurements were performed in the experiment described above and showed a good correlation of HCO concentration distribution with model predictions [170]. However, comparable information can be obtained when the product of OH and CH_2O concentrations is assessed [171]. It has been shown from calculations that this product compares well with the local heat release rate. Since both quantities can be measured in unsteady systems on a single-shot base, this gives an opportunity to measure heat release and thus the exact position of the flame front in turbulent combustion processes.

Multiscalar measurements of turbulence-chemistry interactions rely on a variety of Rayleigh, Raman and LIF techniques [172]. Flashlamp-pumped dye lasers, due to their long pulse length, provide high energy pulses ideal for Ra-

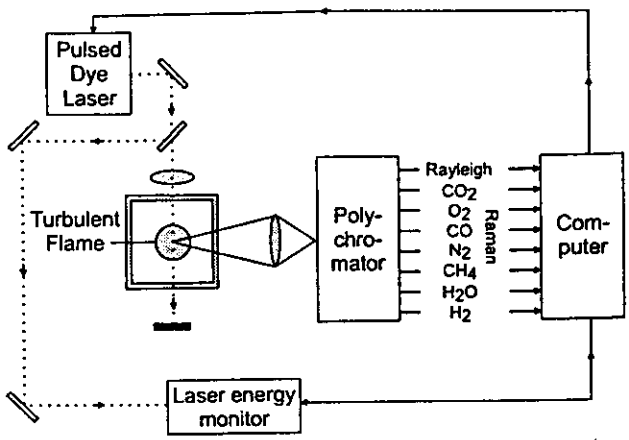

Fig. 30. Experimental setup for pointwise measurements of concentrations and temperatures in flames by Raman and Rayleigh spectroscopy [173-176].

man and Rayleigh measurements. Because of their low average power density, high signal levels can be obtained without inducing air breakdown. Spectrally resolution of the signal yields simultaneous information (Fig. 30) about the concentration of the major species and the local temperature [173-176]. These laser systems used in the intracavity configuation have also been applied successfully to two-dimensional Rayleigh and Raman imaging [177], which has been used to measure temperature and mixing ratio distributions. On the other hand, the long pulses produced by flashlamp pumped dye lasers may be disadvantageous when investigating highly turbulent flows. Other studies using KrF excimer lasers for excitation have been applied successfully to Raman measurements in hydrogen/air flames [178, 179]. Due to the wavelength dependence of Raman cross sections, signal intensities are significantly higher. However, when applied to hydrocarbon flames, strong fluorescence may be induced, which interferes with several of the Raman signals. Thus polarization techniques [156] have been applied to separate the Raman signal, taking advantage of the fact that Raman scattered light, upon excitation with polarized laser light is not emitted isotropically, in contrast to the fluorescence signal. When using Nd:YAG lasers, due to the relatively short pulse duration, air break-down limits are rapidly met. Detailed multiscalar measurements are thus reported, using pulse-stretching techniques [180]. Combination of this Raman/Rayleigh system with three different LIF systems was installed in the Sandia CRF, detecting OH, NO and CO. These fluorescence data can be evaluated quantitatively using temperature and species data derived fom the Raman measurements, enabling corrections for temperature and quenching effects. Conditional statistics using these multiscalar point measurements in comparison to modelling results reveal significant differences in several cases yield an improvement of model assumptions. OH [181] and NO [182] concentrations, e. g., have been shown to differ systematically from flamelet predictions. Revealing the structure of turbulent flames has found increasing interest and was addressed using laser imaging of temperature, mixture fraction and reactive radicals such as OH [183, 184], CH [169, 185] and HCO [170]. Simultaneous measurements of these quantities, yielding scalar dissipation rates, are critical for the validation of turbulent combustion models describing molecular mixing and extinction processes. Simultaneous measurements of Rayleigh scattering and fuel Raman imaging provides information about temperature distribution and mixing [186]. Both can be used to further quantify e.g. OH LIF data by correcting for temperature and collisional quenching effects [184] (Fig. 31).These measurements showed the correlation of reaction zone width and jet Reynolds numbers and addressed the influence of local dissipation rate on flame extinction.

Three-dimensional representations of concentration distributions [187-189] yield additonal information on the turblent combustion system. Simultaneous flow field measurements using particle imaging velocimetry (PIV) and planar LIF measurements have been presented for a number of species. The concentration dis-

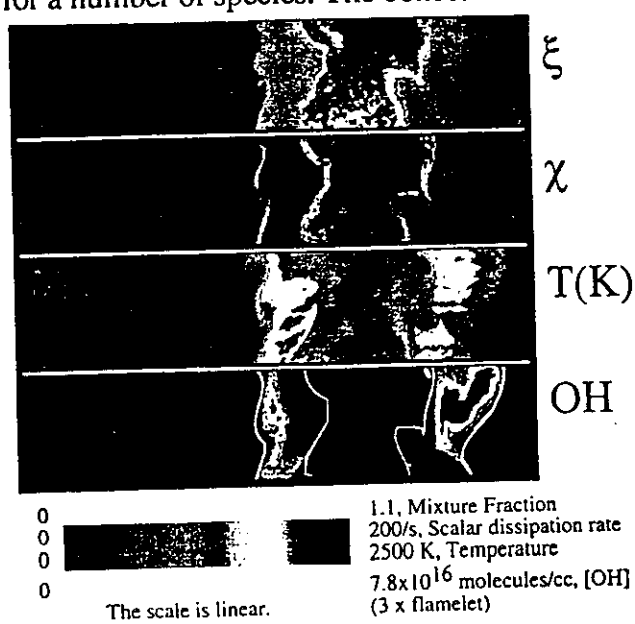

Fig. 31. Images of mixture fraction (ξ), scalar dissipation rates (χ) temperatures and OH concentrations in turbulent CH4/air diffusion flames obtained by 2D Raman, Ralleigh and LIF spectroscopy [184].

tributions of biacetyl, OH and CH have been measured together with the underlying flow fields using LIF [190,191] giving a localization of the instantaneous flame front position. The measurements of flame fronts embedded in the flow field gives valuable insight into the interaction of turbulence and chemistry. Flows seeded simultaneously with molecular tracers (biacetyl) and particles have been used for studying differential diffusion. Since particles have diffusion coefficients of essentially zero, particle distribution yield information about turbulent diffusion. On the other hand, the biacetyl distribution is affected by both turbulent and molecular diffusion. Differences in biacetyl and particle concentration can thus be attributed to molecular diffusion [192].

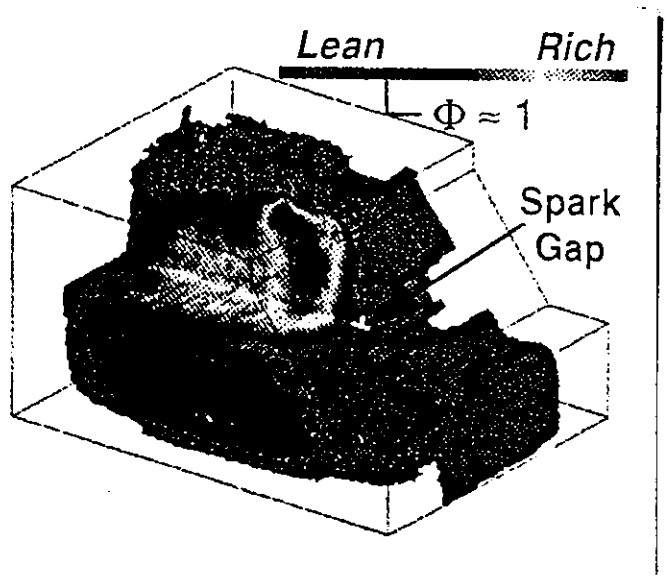

Fig. 32. 3D LIF images of average fuel distribution in a two-stroke direct-injection stratified charge gasoline engine [193].

Engine Combustion

Laser techniques are widespread in modern investigations of internal engine combustion. These studies illuminate different aspects of mixture formation, droplet and spray characteristics, flow dynamics, temperature and species concentration as well as pollutant formation (nitric oxide and soot) and emissions of unburned hydrocarbons. Many of these data, acquired experimentally in technical systems, are used to validate and improve combustion models that are frequently applied in the development of engine design.

Mixture formation

Fluorescent diagnostic systems, based on the photophysics of organic molecules and intended for PLIF measurements of fuel distribution, mixing, evaporation, and flow visualization have been developed. Fluorescing molecules interact with their surroundings, either by concentration-dependent effects like quenching or physical effects like temperature and polarity. Commercial standard fuels contain a number of strongly fluorescing aromatic compounds which can easily be used for qualitative imaging of mixing and fuel distribution. Relying on this "natural fluorescence" provides a method of qualitatively visualizing fuel distributions in technical systems. This method has been applied to detailed studies of crevice release and mixture formation in a two-stroke direct-injection engine [193].

However, as a result of different quenching properties of the fluorescing compounds and significant changes in fuel composition with time due to different volatilities, commercial multicomponent fuels are not suitable for quantitative measurements. When using non-fluorescing fuels, well-defined fluorescing dopants can be used to quantify the fuel concentration as long as the vaporization properties of fuel and tracer are reasonably matched. To be sure that the fluorescent dopant evaporates at the same rate as the fuel, a tracer molecule of appropriate size and polarity has to be selected. Carbonyl components exhibit a much lower sensitivity to oxygen quenching than aromatic compounds [194,195]. Therefore the use of carbonyl components like acetone and 3-pentanone is becoming increasingly widespread as a diagnostic tool for mixing in both reacting and non-reacting flows [196-198]. However, for quantitative measurements of the tracer concentration, the photophysical background has to be understood. It has been shown that the absorption spectra shift with temperature, resulting in temperature-dependent fluorescence intensities at fixed excitation wavelengths. Furthermore, pressure dependencies are not yet fully understood. Photophysical models are on the way [199], but to date cannot fully explain all experimental findings. However, the temperature dependence of ketone fluorescence offers the opportunity to measure gas-phase temperatures [195, 200, 201] in the range up to 1000K, which are the relevant temperatures prior to ignition in IC combustion.

For simultaneous measurements of the fuel distribution between liquid and gas phase and for quantitative measurements of fuel vapor distribution in the presence of droplets, Melton invented the use of a exciplex-based systems [202]. A combination of TMPD (NNN'N' tetramethyl-p-phenylenediamine) and naphthalene

as tracer pair is used. This method is frequently used for qualitative imaging of spray evolution and evaporation in technical applications [203] and has been shown to be valuable in evaluation of engine designs. Due to the high boiling points of the mentioned tracers (above 200°C), significant changes of concentration during fuel evaporation may occur. Triethylamine and benzene as tracer pair [204] match the boiling point of iso-octane which is frequently used as non-fluorescing standard-fuel.

Studies of the mixture formation in IC engines, including a variety of majority species like oxygen, fuel, nitrogen and water, were also performed using Raman scattering (Fig. 33). Spectrally resolving the Raman signal emitted from a line through the combustion system yields one-dimensional concentration distributions of majority species [205]. Using this setup, studies of cold-start behavior, mixture formation and exhaust-gas recirculation are feasible in realistic engines. Since signals can be transmitted via optical fibers, optical access can be provided using extremely small windows enabling studies in realistic engines.

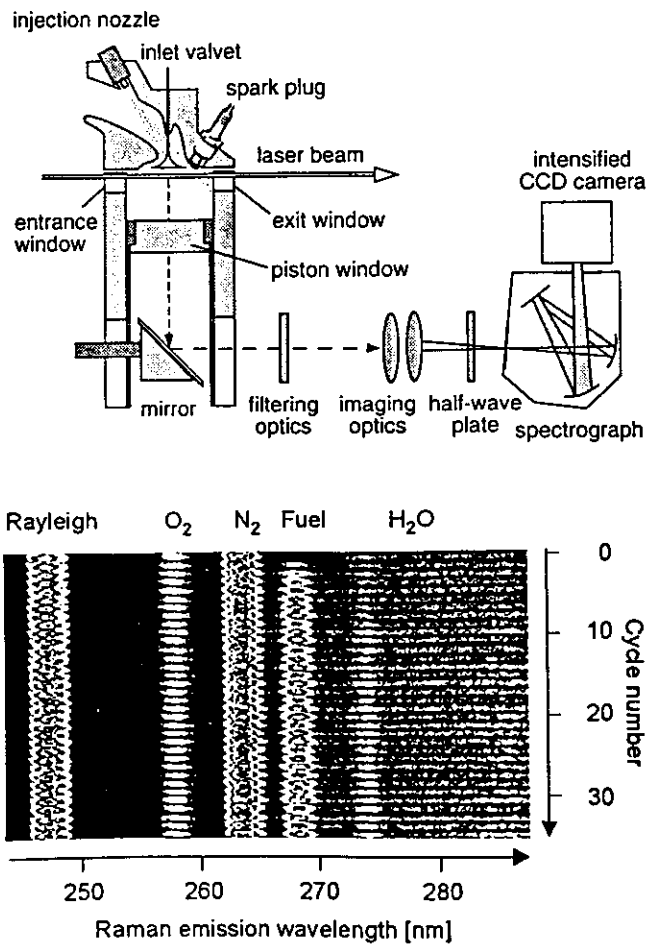

Fig. 33. Experimental setup and signals from Raman scattering measurements in an IC engine [205].

In Diesel engines running on model fuels, 2D Rayleigh scattering has been used successfully for quantitative measurements of fuel distribution [206].

Droplet diagnostics

Design of gas turbine combustors and direct-injection IC engines requires exact knowledge of the evaporation and heating behavior of fuel sprays. Attempts to model heat transfer and evaporation as well as local concentrations within droplets have led to numerous laser studies of isolated droplets under well-defined high temperature ambient conditions. The properties of fuel sprays directly affect performance and emission characteristics of the engines.

Shear-induced internal circulation in droplets increases the rate of heat transfer and, thus, evaporation in contrary to the slow thermal diffusion in the liquid phase. Fluorescence-quenching imaging was performed to elucidate these circulation-induced processes. Ratioing the fluorescence intensity for droplets falling in pure nitrogen and in oxygen-containing atmospheres respectively yields characteristic structures. From these "streamlines" of oxygen quenching, information about internal circulation could be inferred [207].

The spherical or nearly spherical nature of droplets provides several unique optical features. Thresholds for stimulated processes like lasing or stimulated Raman scattering within droplets may be reduced by some orders of magnitude if compared to bulk liquids. Additionally, the spectra emitted from droplets show unique features due to the presence of optical cavity resonances [208]. From the mode structure of the emitted fluorescence light, droplet diameters can be obtained [209]. Distinguishing between fluorescing and lasing droplets or liquid ligaments using the different colors of emission provides a technique for discriminating between droplets of different symmetry and size at a given input-laser intensity [210]. Another attempt to gain information about the evaporation history of droplets was made by Stepowski et al. [211], using fluorescing non-volatile tracers (rhodamin dyes) as markers for the liquid phase. Since the dye concentration rises with the evaporation of the fuel, fluorescence intensity yields information about the initial size of the droplets. The actual size was obtained from Raman imaging. Two-dimensional imaging of droplet size distributions is possible using a combination of fluorescence and Mie scattering techniques [212]. The results of a variety of different laser sheet techniques enabled Dec [206] to develop a 'conceptual model' of Diesel com-

bustion. The synopsis of the results of techniques yielding information on liquid fuel distribution, vapor-fuel/air mixing, PAH distribution, soot concentrations and size distributions, flame structure measurements and localization of autoignition sites yielded a model for diesel combustion which differs significantly from what was thought before laser techniques were applied.

Flow fields

Single point measurements [213] are the simplest and most common techniques for flow characterization. Light sheet techniques for two-dimensional flow field measurements, such as particle-tracking anemometry (PTA) [214] and and particle-imaging velocimetry (PIV) [215,216], yield the two-dimensional projection of the flow velocities to the illuminated plane. Both techniques require a multiple measurement of particle positions using illumination with a thin pulsed lightsheet. Subsequent data analysis calculates the local velocity from the displacement of the particles. Detection of small velocities requires high resolution of the individual images. Due to the availability of high resolution CCD camera systems and fast computers today, real-time analysis of flow systems is feasible. Using dual-pulse, single-frame techniques leaves an ambiguity in direction. This can be overcome using an unequally spaced third pulse [217] or specialized dual-imaging cameras which allow for the detection of two separated images with short temporal delay. Detailed studies of flow fields in an optically accessible research engine have been presented by Köhler et al. [218]. Doppler Global Velocimetry (DGV) [219], like LDA, makes use of the Doppler shift of scattered light from particles having velocity components relative to the direction and detection of the laser beam.

Particle seeding can be avoided using flow tagging by vibrational excited oxygen [220] or by photodissociating water and subsequent laser-induced fluorescence detection of OH [221] have been demonstrated. The oxygen tagging technique (RELIEF [222]) takes advantage of the relatively long lifetime of vibrational excitation of homonuclear molecules.

Temperatures

Laser-based, non-intrusive techniques used for thermometry include LIF, Rayleigh and Raman [223] scattering, CARS [224] and DFWM [225]. Since Raman techniques require a spectral dispersion of detected signal light, one-dimensional measurements along a laser-illuminated line within IC engines are feasible [156]. For two-dimensional imaging of temperature distribution, Rayleigh scattering is frequently used [226-228] in systems where pressure inhomogeneities are negligible. However, the application of diagnostics using elastic scattering requires additional care in the optical setup since the signal is not spectrally shifted towards the excitation wavelength. Since Rayleigh scattered light emitted from the gas volume under study is Doppler broadened, a narrow-band excitation source filtered Rayleigh techniques can be used to suppress the narrow-band contribution of scattered light from surfaces and windows [229].

Pollutant formation

The following discussion focuses on NO, which is, with soot and unburned hydrocarbons, one of the major combustion-related pollutants in engine combustion. Despite the development of improved exhaust-gas aftertreatment systems, it is necessary to investigate possibilities to reduce the formation of nitric oxide already during the combustion process itself, especially in view of very lean burning engines, where catalytic converters are difficult to operate. Various strategies using different laser excitation wavelengths, laser sources and fluorescence detection bands were investigated as tools for in-cylinder engine NO diagnostics. NO concentration measurements in spark ignition (SI) and Diesel engines, exciting NO with tunable ArF excimer lasers at 193 nm (ε-bands) [197, 230] and at 225 nm (γ-bands) using the Raman-shifted output of tunable KrF-excimer lasers [231], are reported. However, to circumvent the strong attenuation of these short excitation wavelengths in many technical combustion systems, excitation of NO with tunable KrF excimer lasers at 248 nm was suggested [232]. Since then, this technique has frequently been applied for quantitative measurements of NO in IC engines [233-235]. This detection scheme was characterized by measurements in stabilized high-pressure flames [233]. The excitation laser is tuned to the O_{12}-bandhead of the A-X(0,2)-transition where the fluorescence excitation spectrum of molecular oxygen has a local minimum (Fig. 23). NO fluorescence emitted in the A-X(0,1)- and A-X(0,0)-bands at shorter wavelengths is detected, which further minimizes the influence of interferring species. Attenuation of signal light is weak as long as the illuminated volume is close to the detection window and, thus, the optical path length through the burned gases at high pressure is short. Quantification of LIF signal intensities requires detailed knowledge of several temperature- and pressure-dependent factors. Variation

of absorption spectra due to line broadening and shifting [236] changes the spectral overlap of laser profile and absorption line [237]. To account for the effect of collisional quenching, data obtained for many combustion-relevant colliders are available [238-240]. Using modelling results for the change of mixture composition around the flame front, local quenching rates were calculated [231]. The temperature dependence of quenching rates in the burned gas region for equilibrium gas compositions has also been presented [235]. The collisional quenching rate scales linearly with pressure, and is a function of temperature and gas composition. It turns out, however, that behind the flame front, i.e., the region where NO is predominantly formed in engines, the quenching rates are nearly constant due to compensation effects of composition changes and temperature. Using these results, detailed comparisons of NO concentration profiles obtained from different measurement approaches and modelling results were shown [241]. Quantitative results are usually obtained by calibrating the overall detection efficiency. In the case of NO, calibration is possible by doping known amounts of NO to the burn gases [235]. The simultaneous application [233] of Rayleigh scattering and LIF for measurements of temperatures and NO concentrations in an internal combustion engine is shown in Fig 34. From the image pairs with corresponding NO concentrations and temperature fields it can be seen that NO is formed in high temperature areas. While the overall spatial distribution of NO and temperature is strongly correlated, the profiles

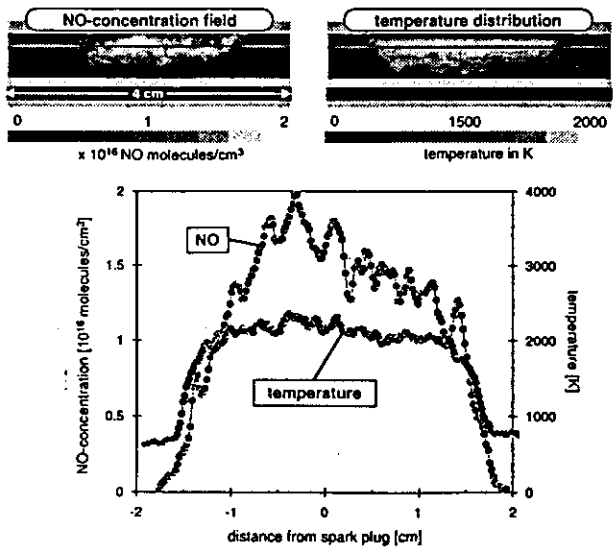

Fig. 34. Simultaneous single-shot absolute NO concentration and temperature fields in a transparent SI engine fueled with propane/air ($\lambda = 1$) using 2D LIF and Rayleigh scattering [233].

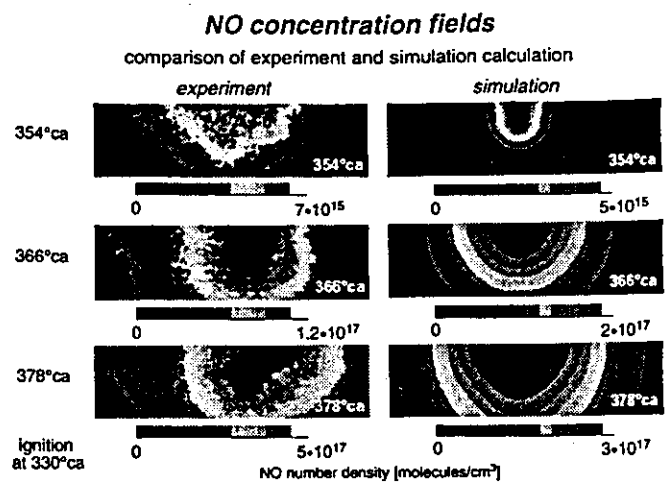

Fig. 35. Measured (2D-LIF) and calculated NO concentrations in a horizontal plane 5 mm above the cylinder gasket in a single-cylinder IC engine [244].

in Fig. 34 indicate that the temperature distribution is more uniform than the NO concentration distribution. Due to the strong non-linear temperature dependence of the NO production rate, careful control and homogenization of the combustion conditions should allow reduction of primary NO formation. A combination of measurements in a commercial gasoline engine and CFD modelling is presented in Fig. 35. The in-cylinder flow field was measured (PIV), whereas the temporal evolution of the NO concentration fields was observed for different planes and operating conditions [235] together with temperature measurements from OH two-line thermometry [242] and a new temperature imaging technique using indium atomic fluorescence [243]. Mean flow characteristics and the flame front development were predicted with good accuracy. Calculated NO concentrations compared well with the experimental result in respect of spatial distribution and absolute numbers [244].

Laser-based Combustion Control

To reduce the environmental effects caused by stationary combustion of fossil fuels, efficient control strategies are needed to optimize the process with regard to pollution emission, specific energy production and overall cost of the process [245]. These improvements call for fast active control loops based on sensors for species concentration,temperature, flow and other process parameters. Apart from sufficient sensitivity, selectivity and response times a sensor suitable for industrial process control applica-

tions has to offer important additional features like compactness, long sensor life time, good long term stability, reliable and simple calibration, ease of use, and finally low cost of ownership with respect to the possible savings in the process. As proven in many laboratory applications laser absorption techniques have a unique potential with regard to selectivity, resolution and speed. The possibility to measure over large distances avoids the numerous disadvantages of sensors based on local measurement principles or extractive probe sampling especially in chemically aggressive, high temperature or high pressure combustion environments.

The important question, if laser sensing can be transferred from a valuable lab technique into an industrial control tool, is closely connected to an adequate choice of the laser source. While for sensitivity and selectivity reasons the fingerprint region in the infrared (2-20μm) is most interesting for species sensors, the lack of infrared lasers suited for the industry prevented wide spread use. Due to tuning restrictions neither CO_2 ($\lambda \approx 10{,}6\mu m$) nor the IR-HeNe (3,39μm) lasers are real alternatives, since their usability for gas sensing depends on accidental coincidences with strong absorption lines. Nevertheless the high output power and the multitude of CO_2-laser lines allowed some important sensing applications of hydrocarbons, ammonia and other species [246-248] and led to one of the first commercialized industrial grade species sensors for closed-loop control applications: a laser **in situ** ammonia sensor named LISA [249,250] used for optimization of NO_x - removal in the SCR or SNCR-process. Due to coincidences with strong C-H-stretch rovibrational transitions of most hydrocarbons [251] the IR-HeNe laser is used frequently for CH_4-monitoring [252.253]. Combined with recently available infrared transmitting fibers a robust but sensitive absorption based sensor was developed which could be be used to study local mixing effects in CH_4-combustion [254] with up to 2kHz time resolution and relative sensitivities of 4% in CH_4 mole fraction (Fig. 36). Under lean conditions small levels of unmixedness can cause a dramatic increase of NO_x-formation due to the nonlinear equivalence ratio dependence of NO_x production.

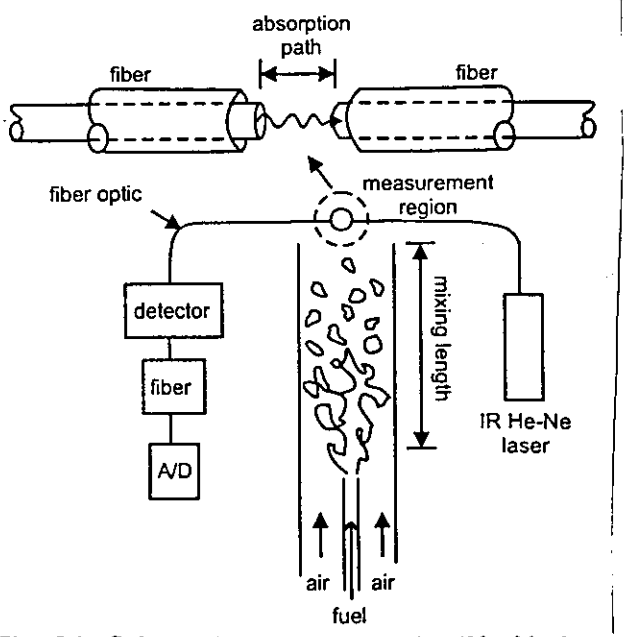

Fig. 36. Schematic of optical probe (He-Ne laser at 3.39 μm) for CH_4-mixing studies in a modified Karlowitz burner [254].

The laser near perfectly suited for industrial sensor applications is the near infrared, room temperature diode laser (NIRDL), which is available with almost complete spectral coverage from 635 to 1650 nm. Developed for communication technology together with high performance detectors and glass fibers they are produced in enormous quantities. With regard to industrial sensors they offer a unique combination of positive properties like low cost, tiny size, room temperature operation, laser lifetime of 10^5 hours and more, single mode output power of up to several 100 mW, and excellent spectral resolution of 10^{-3} nm. Most important is their fast and continuous tunability by current modulation ($>10^5$ GHz/s over 30-100 GHz) and the possibility to acquire a complete absorption line shapes allowing either a simplification of the signal interpretation or by evaluation of the spectral line profile the simultaneous extraction of physical boundary conditions (pressure, temperature, velocity, mass flux and others) in the measurement volume. Their major disadvantage to cover only relatively weak transitions in the visible and near infrared range(e.g. overtone and combination vibrational bands, magnetic dipole transitions, line strength 10^{-23} to 10^{-21} cm/molecule) is not as important for many process control applications since mostly major species have to be monitored (CH_4, O_2, H_2O, CO_2). Even simultaneous detection of multiple species within the same measurement volume can be realized fairly comfortable by fiber-multiplexing multiple diode lasers in a single fiber [255-258] taking advantage of their small size, low cost and capability for fiber delivery in high quality fibers. Crosstalk between the species channels is avoided by wavelength-multiplexing or time-multiplexing of the specific absorption signals. The absorption signals are acquired in the wavelength-multiplexed case by simultaneously scanning all lasers and dispersing the

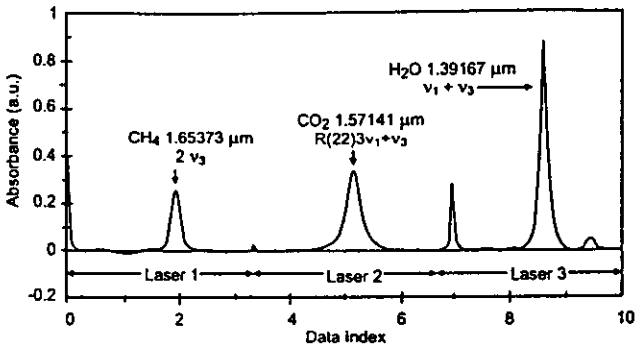

Fig. 37. Example for a near simultaneous multispecies detection of CH_4, CO_2, and H_2O by sequentially scanning three independend diode lasers (time multiplexing) [260].

multiwavelength beam after passage of the absorption path onto multiple detectors by use of a grating [255-258] or dichroic beamsplitters [259]. Time-multiplexing means sequentially scanning each laser using only a single detector [260] as shown in Fig. 37 for the near simultaneous (within 10 ms) detection of CH_4,CO_2,H_2O in a single pass cell using a three diode laser sensor operating at 1.65, 1.57, and 1.38 µm [260]. Up to now multiple species detection is mostly done with several diode lasers due to scan range limitations of monolithic lasers. However recent progress in external cavity diode lasers [261,262] and multisection distributed feedback (DFB)- and distributed Bragg-reflector (DBR)-lasers [263,264] continuously scanning up to 100 nm will simplify spectrometer design significantly. Summarizing all that it will be shown in the following examples that NIRDLbased absorption sensors are most promising for wide area of control applications ranging from mobile and though severely space restricted sensors (like inflight or portable sensors, or vehicles exhaust probes), over fast non-intrusive in situ temperature sensors working in hostile high temperature [259] and high pressure [265] environments (flames, plasmas, gaseous combustion) to ultimately industrial "real world" applications like full scale waste incinerators.

For improved propulsion control of advanced flight vehicles rapid-response in situ air mass flux sensors are needed which do not disturb the flow field downstream the measurement location in the turbine inlet. Optical mass flux sensors determine the density velocity product of a gas flow by simultaneously inferring velocity from the Doppler-shift of the line profile and density from the magnitude of the scattering or absorption signal [266-269]. The low power requirements of absorption techniques in combination with diode lasers and glass fibers give an ideal choice for robust inflight sensors with tremendous advantages in space, weight, cost and stability. These could be exploited by using O_2 as a flow indicator molecule [270] which is present in a high, known and constant concentration and detecting it near 763 nm via the magnetic dipole transition O_2 (b-X) (0-0) [271]. Adapting a concept originally used in shock tube experiments [272,273] (Fig. 9) the weak, Doppler-shifted O_2-absorption along two angled absorption paths across the inlet duct of a full scale Pratt&Whitney F-100 engine (Fig. 38) could be used in ground tests (in flight experiments on a research F-18 aircraft are in preparation for 1998) to determine air densities, gas velocities (up to 160 m/s with 0.4 m/s resolution) and mass flux with an accuracy of 1-2% at a time resolution of about 1 s over the full range of engine operating power [270], thereby demonstrating the potential of diode lasers to provide compact and robust sensor solutions for extreme working conditions.

The considerable advantages of optical tempe-

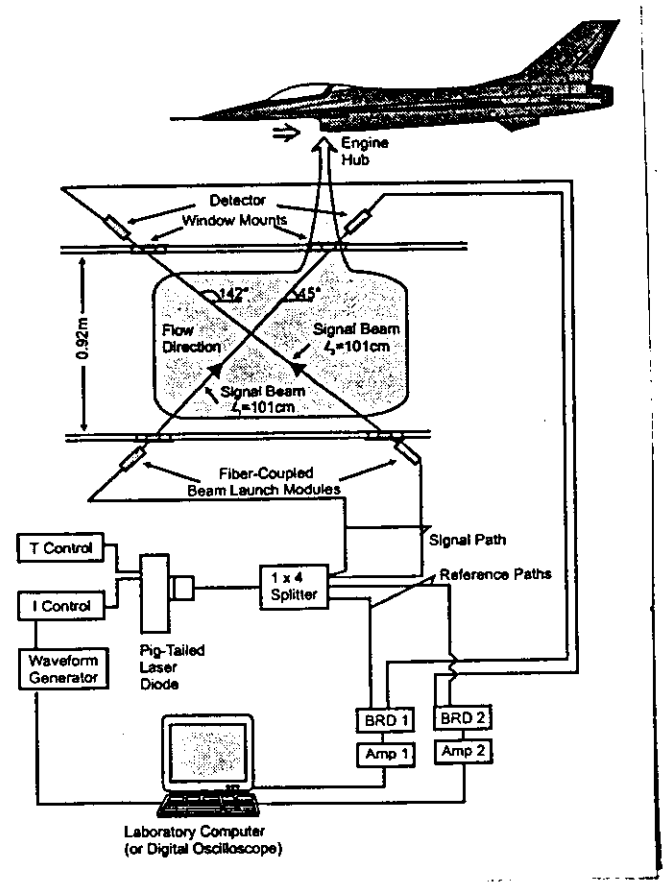

Fig. 38. Schematic layout of a diode laser based air mass flux sensor using O_2(b-X) (0-0) [271] transition to determine air densities, gas velocities and mass flux with an accuracy of 1-2% at a time resolution of about 1 s at a Pratt&Whitney F-100 engine [270].

rature measurements over intrusive standard techniques like thermocouples with regard to robustness and measurement speed promise improved monitoring and control of heat release in high-temperature process streams. This was recently put into action for gaseous combustion by Hanson et al. for the case of an active closed-loop temperature control of a small laboratory Hencken-burner [255] and for an automatic closed-loop process optimization of a pulsed 50-KW model incinerator [274]. In both cases temperature was inferred by ratioing two H_2O transitions, employing a fiber-coupled, multiplexed dual diode laser system. Since water is present in high concentrations in all hydrocarbon combustion processes and has a strong rovibrational absorption band around 1,4 µm it is an ideal molecule for temperature measurements and very well suited for a detection by NIRDL. By extracting the temperature from the ratio of the peak absorption coefficients instead of a fit to the line profile a time resolution of 100 µs could be achieved. Probing the post flame gases of the Hencken-burner (diameter 7 cm) with an earlier version of this setup temperature fluctuations up to 250 Hz could be resolved and used to control the flame temperature by adjusting the fuel flow via a computer based closed-loop feedback circuit.The closed-loop performance of this system in response to a step change in fuel flow rate is depicted in Fig. 39. With a response time of the closed-loop control system of ≈10 msec, which was primarily limited by the the gas residence time in the burner, the gas temperature in the probed region could be controlled within a relative standard deviation of 1% of the desired value for set points around 1950 ±150K (Fig. 40). Getting closer to industrial scale systems the temperature sensor could be used in an improved version to probe the flue gas duct (diameter 18cm) of a pulsed 50kW model incinerator and use the in situ temperature fluctuations

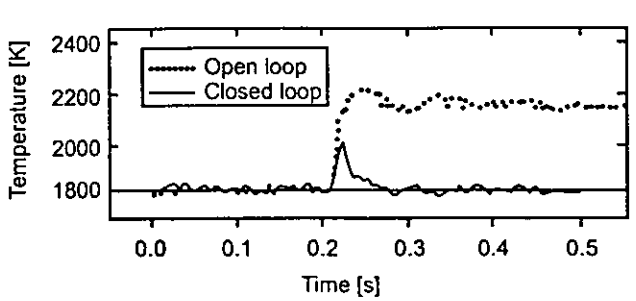

Fig. 39. Closed and open loop(no feedback) performance of a diode laser temperature sensor with respect to a step change in the fuel flow rate of a Hencken-burner (Ø7 cm) [255].

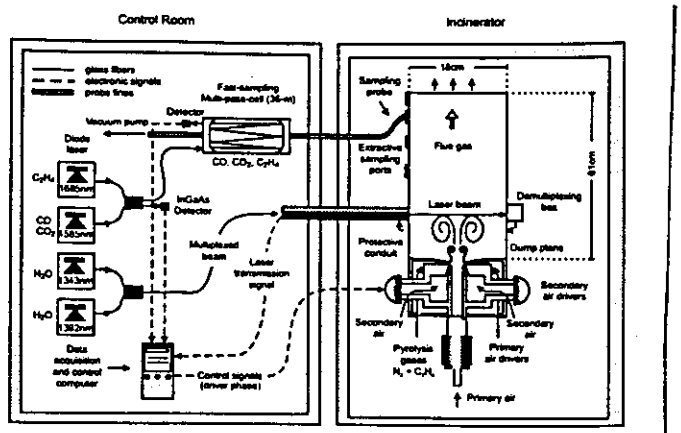

Fig. 40. Closed-loop control of a pulsed 50kW model incinerator using a multiplexed fiber-coupled multi-species diode laser system for the in situ detection of temperature and H_2O and fast-sampling detection of CO, CO_2, and C_2H_4 [274].

(T_{RMS}) to optimize the relative phase angle ϕ between the primary and secondary air injection pulsed at identical frequency f_0. As depicted in Fig. 41, mixing, CO emissions and temperature fluctuations at f_0 are controlled by the phase angle. Compared to using no or only primary air forcing CO-emissions can be reduced from 2500 ppm resp. 800 ppm to below 200ppm with phase optimized secondary and primary air forcing.To use T_{RMS} as a control variable to minimize CO emissions and ensure complete fuel oxidation the 183 Hz T_{RMS} component had to be extracted with sufficient accuracy and resolution. Temperature time histories of one second and measurement rates up to 10 kHz were required which are hardly possible by

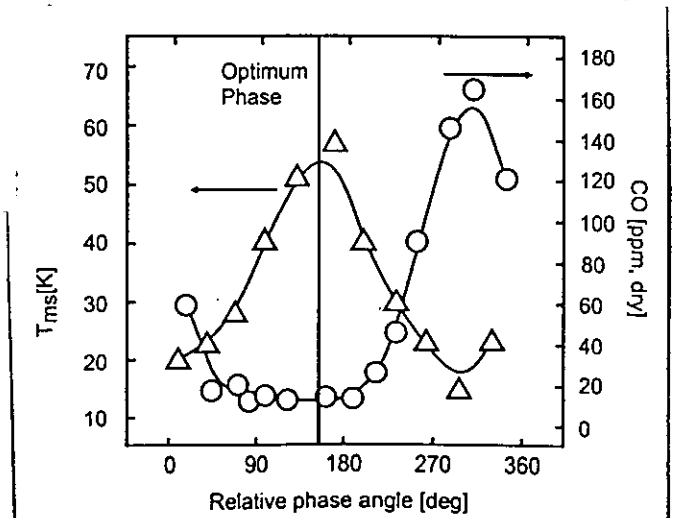

Fig. 41. Dependence of the control signal T_{RMS}, measured in situ in a pulsed incinerator [274] , and the CO concentration, determined extractively, on the phase angle between the primary and secondary air driver (Fig. 40).

alternative methods. Using T_{RMS} as a sensor signal to optimize the phase angle with this set-up a computer-controlled closed-loop optimization from an arbitrary starting position within about 30 control steps (10 sec each, limited by data transfer and computation speed) was possible.

The transition from a prototype instrument to a permanent industrial application imposes many restrictions on sensor setup and design. Particularly the sensor scale-up of in situ techniques to accommodate industrial process dimensions intensifies minor disturbances hardly known in a lab-scale experiment to severe complications, so that the necessary efforts only pay off for processes with a high return of investment or a high demand for on-line control such as waste incineration. Large variations in composition, calorific value and humidity of the waste call for a precise on-line control of grate movement, fuel and primary /secondary air input to enable complete combustion and guarantee the desired heat release (Fig. 42). The SNCR-system also needs a sensitive adaption of Urea/NH_3 -injection to minimize additive consumption and ensure 90% NO_x removal. The SNCR is actively optimized by an CO_2-laser based in situ ammonia monitor (LISA) [249,250], while primary air injection, grate movement and fuel input are under closed-loop control through an IR-scanner-camera (TACCOS)[275] measuring the waste bed temperature. Secondary air control to achieve a constant air ratio is under construction by NIRDL-based in situ detection of O_2 at the end of the secondary combustion zone. In a gas cell NIRDL-based O_2-detection is possible with a sensitivity of 20 O_2-ppmV· m [276]. The same task presents a major problem if performed inside a full scale incinerator since the molecular absorption is sometimes orders of magnitude smaller than the numerous disturbances which interfere with the signal. Most important are changes in the effective transmission of the in situ path which can be caused by the quickly fluctuating dust load of the flue gases, destruction and contamination of windows and other optical surfaces by dust, heat, or chemical attack and by thermal background radiation. Additional disturbances, which are caused by refractive index gradients, thermal lensing, mechanical vibrations, and thermal drift or deformation of the boiler walls, effect the laser beam profile

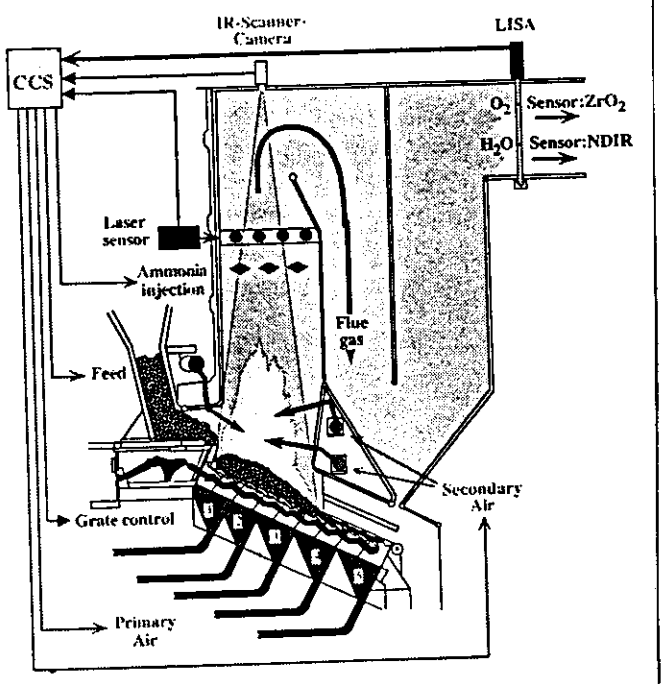

Fig. 42. Intersection through the waste incinerator at which the in situ detection of O_2 and H_2O has been performed. A selection of important sensors (diode laser in situ sensor, laser in situ ammonia sensor, LISA, and IR-scanner-camera, TACCOS) as well as the possible actors which are connected to the combustion control system, CCS, are indicated [259].

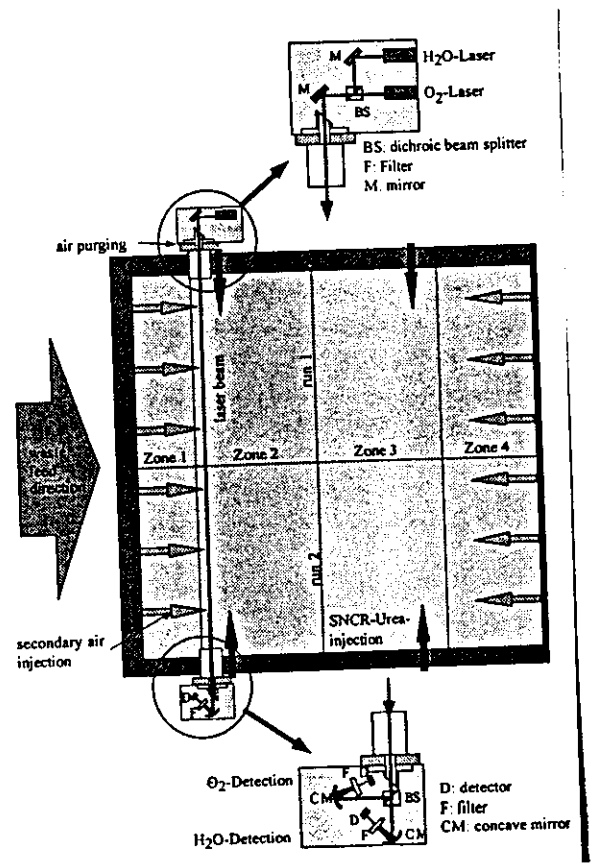

Fig. 43. Outline of the waste incinerator and set-up of the diode laser based dual species in situ spectrometer [259].

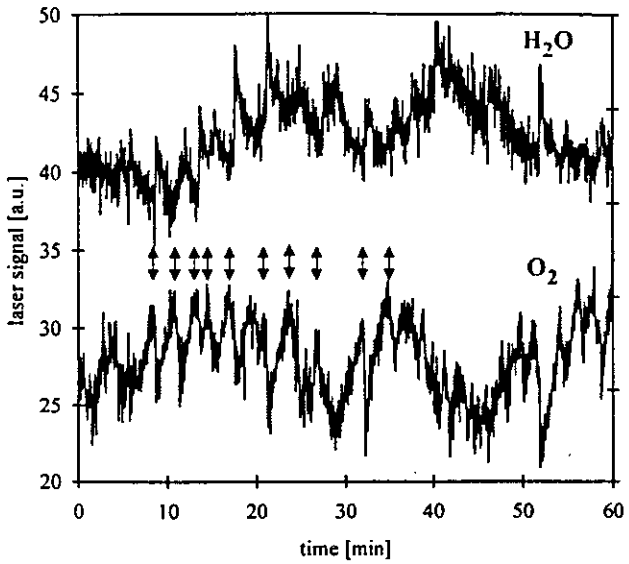

Fig. 44. Simultaneous in situ-detection of oxygen (bottom trace) and water (top trace) in a waste incinerator with diode lasers at 760 an 812 nm over a period of one hour with a time resolution of 1s. On both signals appear quasi periodic fluctuations, which are strongly anticorrelated and caused by the feeding cycle and the grate agitation of the incinerator (marked by arrows) indicating the feeding process and the mixing of the fuel [259].

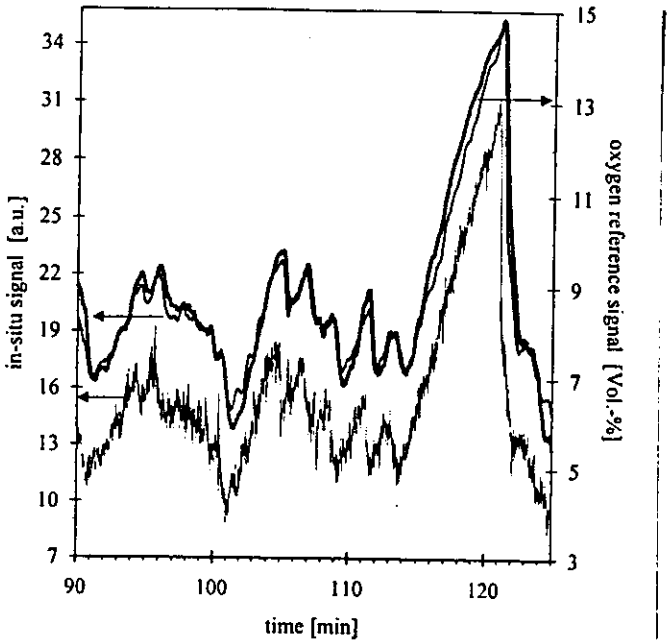

Fig. 45. Comparison of the O_2-laser in situ signal (top trace thin black line: averaged over 15 samples and time shifted by +20sec; bottom trace: original signal i.e. no average, no time shift) and the reference signal from a ZrO_2-sensor (top trace thick line) sampled 45m further down the flue gas duct [259].

or pointing stability and reduce the light collection efficiency and the transmission. Finally all electronic signals and particularly the detector signal can be sensitive to electromagnetic pick up, high voltage and current switching, ground loops, and thermal drift of electronics. To make things worse it has to be noted that the absolute magnitude, frequency and temporal behaviour of all these interferences depend on the specific process and site to be monitored and even on its momentary conditions. Additionally care has to be taken of variations in temperature and concentration along the absorption path and their respective time dependence. Despite all this simple to use, but inexpensive and robust solutions have to be found to suppress, compensate or stabilize all the disturbances over long periods of time in order to allow a permanent signal acquisition and stable control of the process. Many of these problems could be solved so that a simultaneous in situ detection of O_2 and H_2O in a full scale municipal waste incinerator (4m in diameter, 20 MW_{th}) were possible over time periods of days [259]. Using a wavelength multiplexed setup (Fig. 43) with air purged windows to avoid transmission degradation, wavelength modulation at a frequency well above the transmission noise caused by dust fluctuations, optical narrowband interference filters to suppress thermal background radiation, an analog electronic circuit for a fast on-line transmission correction, low-pass filtering of the raw signal to suppress electronic noise, and a fast fitting routine to provide line locking signals and to extract the concentration from the digitized and averaged absorption profile we achieved a simultaneous detection of O_2 and H_2O at 760 nm/818nm with a sensitivity of about 0.3 Vol% and a temporal resolution of 1s. As depicted in Fig. 44 the expected close temporal coupling between O_2-consumption, H_2O-production and grate agitation or fuel feed -indicated by arrows- could be shown experimentally. The laser signals were compared to extractive reference sensors, a nondispersive IR-sensor with a heated probe line for H_2O and a ZrO_2 sensor for O_2, which probe the relatively cold flue gases 45 m behind the laser measurement location(see Fig. 42). After removal of time offsets, caused by the gas transport to the extractive probe, and low pass filtering of the in situ signal to match the response time, reference and in situ signals showed very good agreement (Fig. 45 for O_2). This indicated clearly a good linearity and allowed an absolute calibration of the in situ signals. The high time resolution and the fact that the in situ signals are faster by 30 s for O_2 and 60s for H_2O than the reference signals, since the gas transport could be avoided, are the main advantages of the in situ signals which make them very attractive for

control purposes.

The need for a significant reduction in CO_2-emissions from coal combustion requires the development of new concepts for increasing the efficiency in the conversion of solid fuels . An increase in efficiency - over 50% - is feasible in a combined plant, in which an additional expansion turbine is included after the main combustion chamber. However, a major issue in this area is the removal of alkali compounds, which is particularly acute in pressurised systems, where the flue gas has to be cleaned hot. Alkali vapors generally pass through conventional filters since they are present as gaseous or fine aerosols. Corrosion damage at the entrance to to turbines is feared even at ppb levels. On the other hand, for coals with high alkali and chlorine content, and for high combustion temperatures (1300-1500°C), quantities of alkalis in the flue gas may reach even ppm levels. Thus a dynamic range of several orders of magnitude combined with a high time resolution is needed. Since alkali vapours interact strongly chemically with metallic materials only an on-line and in situ laser technique can eliminate the sources of error of sampling measurements. Recently, several novel on-line techniques have been developed for monitoring alkali species in industrial situations. One of these, excimer laser induced fragmentation fluorescence (ELIF) is sensitive essentially only to gas phase species. The method uses excimer laser light to simultaneously photodissociate alkali compounds of interest and excite electronically the alkali atoms formed. Fluorescence from the excited Na(3^2P) or K(4^2P) atoms is readily detected in the visible region. The potential of ELIF for combustion diagnostics was first demonstrated by Oldenburg [277].Since then, the method has been applied as a truly in situ optical technique to analyse alkali species in the flue gas of several small-scale coal combustion and gasification systems [278-281]. Measured signals are converted to absolute concentrations using a calibration method that monitors alkali compounds under known conditions of temperature, pressure and composition and using the same optical geometry as at the reactor. Also needed for quantification are data on laser beam absorption, collisional processes etc. [282]. A single-port arrangement (Fig. 41), whereby laser access and fluorescence detection were achieved through the same window, was recently demonstrated for measurements in a pressurised circulating fluidised bed (PCFB) pilot plant. This geometry avoids the requirement for the laser beam to reach across the entire width of the flue gas pipe. It was shown that

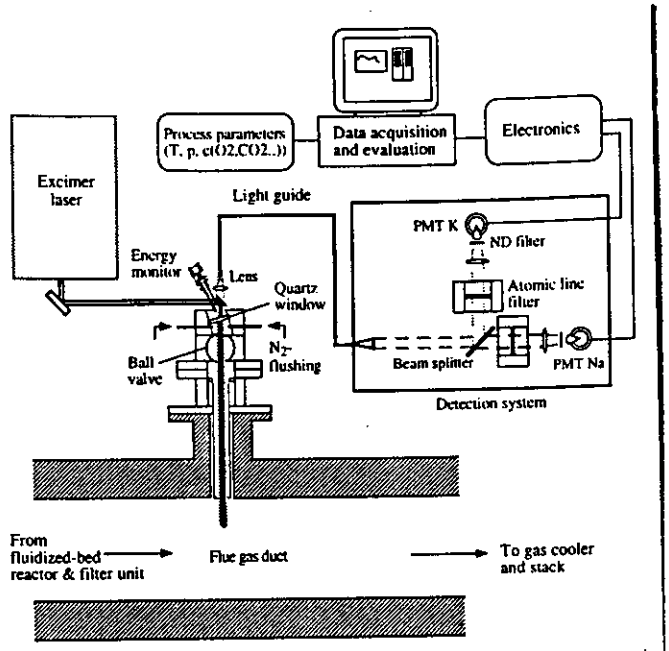

Fig. 46 Detection of alkali species in the flue gas from a PCFB plant with a single-port ELIF system.

alkali concentrations can be monitored continuously over a whole day and responded promptly to changes in reactor conditions. Measured concentrations were also found to vary considerably with coal type (e.g. lignite or hard coal). A detection limit for both alkalis of 0.2 ppb was established at 10 bar total pressure and 800° C measurement temperature. In addition, ELIF is applicable to heavy metal species [283]. Other new on-line techniques for low level alkali detection are plasma-excited alkali resonance line spectroscopy (PEARLS) [284] and surface ionisation (SI) [285]. They are complementary to the ELIF technique in that they are capable of detecting aerosols as well as gas phase alkali species. Thus simultaneous measurements will provide information of the physical state of the alkali species in the flue gas.

Conclusions

After three decades of research and development in the area of laser-based concepts for combustion diagnostics many of the spectroscopic methods have matured now from qualitative to quantitative techniques. Several typical areas of combustion research have been discussed in this paper to present some insight into the powerful possibilities that laser spectroscopy offers in this field.

Acknowledgments

I am grateful to Donald Hardesty and Brian Haynes for the honour of being invited to prepare this lecture. My sincere gratitude goes also to a large number of colleagues who send me most useful material. I sincerely hope that they can accept my apologize for including only a small fraction into this manuscript. Special thanks also to my colleagues and collaborators in Heidelberg Th. Dreier, V. Ebert, P. Monkhouse, C. Schulz, H.-R. Volpp and J. Warnatz for their active collaboration to cut down the enormous material to a manageable size. The generous support of our work by the Deutsche Forschungsgemeinschaft (SFB 123 and 359), the BMBF, the State of Baden-Württemberg (TECFLAM) and the European Commission (JOULE) and many industrial companies is gratefully acknowledged.

REFERENCES

1. Bellomo, R. V. , *J. Human Evolution* 27:173-195 (1994).
2. Hottel, H. C., *Trans. Am. Inst. Chem. Engrs.*, 19:173 (1927).
3. Kirchhoff, G. R. , and Bunsen, R.W., *Poggend. Annal.* 110:161-176 (1860).
4. Ostwald, W. and Bunsen, R. W., *Sammlung Meister 3. Bd.*, Feuer Verlag, Leipzig, 1910.
5. Einstein, A., Mitteilungen der Physikalischen Gesellschaft Zürich. Nr. 18 (1916); *Phys. Z.* 18:21-128 (1917).
6. Gordon, J. P. and Townes, C. H., *Phys. Rev.* 99:1264-1274 (1955).
7. Maiman, T. H., *Nature (London)* 187:493-494 (1960); Collins, P. J., Nelson, D. F., Schawlow, A. L., Bond, W., Garrett, C. G. B., and Kaiser, W.: *Phys. Rev. Lett.* 5:303 (1960);
Sorokin, P. P., and Stevenson, M. J., *Phys. Rev. Lett.* 5:557 (1960).
8. Schneider, W. E., *Nature*, London, 200:403-404 (1963).
9. Göppert-Mayer, M., *Ann. Phys.*, Leipzig, 9:273-294 (1931).
10. Gaydon, A. G., *The Spectroscopy of Flames*, Chapman and Hall, London, 1957.
11. Nguyen, Q. V., Edgar, B. L., and Dibble, R. W., *Combust. Flame* 100:395-404 (1995).
12. Eckbreth, A. C., *Eighteenth Symposium (International) on Combustion*, The Combustion Institute, Pittsburgh, 1981, pp. 1471-1488.
13. Penner, S. S., Wang, C. P., and Bahadori, M. Y., *Twentieth Symposium (International) on Combustion*, The Combustion Institute, Pittsburgh, 1984, pp. 1149-1176.
14. Hanson, R. K., *Twenty-First Symposium (International) on Combustion*, The Combustion Institute, Pittsburgh, 1986, pp. 1677-1691.
15. Crosley, D. Ed., *Laser Probes for Combustion Chemistry*, ACS Symposium Series 134, American Chemical Society, Washington, 1980.
16. Wolfrum, J. Ed., *Appl. Phys. B* 50 and 51 (1990).
17. Chigier, N. Ed., *Combustion Measurements*, Hemisphere, New York, 1991.
18. Kompa, K., Sick, V. and Wolfrum, J . , Eds., *Ber. Bunsenges. Phys. Chem.* 97 No. 12 (1993).
19. Taylor, A. M. K. P., *Instrumentation for Flows with Combustion*, Academic Press, New York, 1993.
20. Kohse-Höinghaus, K., *Prog. Energy Combust. Sci.* 20:203-279 (1994).
21. Daily, J. W., *Prog. Energy Combust. Sci.* 23:133-199 (1997).
22. Eckbreth, A., *Laser Diagnostics for Combustion Temperature and Species*, 2nd Edition, Gordon & Breach, Amsterdam, 1996.
23. Demtröder, W., *Laser Spectroscopy - Basic Concepts and Instrumentation*, 2nd Edition, Springer, New York, 1997.
24. Ebert, V. and Wolfrum, J., in *Optical Measurements, Techniques and Applications* (Mayinger, F., Ed.), Springer Verlag, Berlin, 1994, pp. 273 - 312.
25. Rahn, L. A., Mattern, P. L., and Farrow, R. L., *Eighteenth Symposium (International) on Combustion*, The Combustion Institute, Pittsburgh, 1981, pp. 1533-1542.
26. Vanasse, G. A., *Spectrometric Techniques*, Vol. IV, Acad. Press, Orlando, 1985.
27. Farrow, R. L., Rakestraw, D. J., and Dreier, T., *J. Opt. Soc. Am. B* 9:1772-1777 (1992).
28. Abrams, R. L. and Lind, R. C., *Opt. Lett.* 4: 94-96 (1978).
29. Teets, R. E., Kowalski, F. W., Hill, W. T., Charlson, N. and Hänsch, T. W. , Advances in Laser Spectroscopy; Proc. Soc. Phot. Opt. Instr. Eng., 113:80 San Diego (1977).
30. Hunt, J.H., Guyot-Sionnest, P. and Shen, Y.R., *Chem. Phys. Lett.* 133:189-192 (1987).
31. Shen, Y.R., *The principles of nonlinear optics*, J. Wiley & Sons, New York, 1984.
32. Warnatz, J., *Twenty-Fourth Symposium (International) on Combustion*, The Combustion Institute, Pittsburgh, 1992, pp. 553-579.
33. Kleinermanns, K. and Wolfrum, J., *J. Chem. Phys.* 80:1446-1450 (1984).
34. Kleinermanns, K., Linnebach, E., and Wolfrum, J., *J. Chem. Phys.* 89:2525-2527 (1985); Bronikowski, M., Zhang, R., Rakestraw, D.J., and Zare, R.N., *Chem. Phys. Lett.* 156:7-13 (1989); Jacobs, A., Schuler, F.M., Volpp, H.-R., Wahl, M., and Wolfrum, J., *Ber. Bunsenges. Phys. Chem.* 94:1390-1395 (1990); Jacobs, A., Volpp, H.-R., and Wolfrum, J., *Chem. Phys. Lett.*

177:200- 206 (1991); Keßler, K. and Kleinermanns, K., *J. Chem. Phys.* 97:374-377 (1992).
35. Buchenau, H., Toennies, J. P., Arnold, J., and Wolfrum, J., *Ber. Bunsenges. Phys. Chem.* 94: 1231-1248 (1990); Michael, J.V., Fisher, J.R., Bowman, J.M. and Sun, Q., *Science* 249:269-271 (1990); Kitsopoulos, T.N. Buntine, M.A., Baldwin, D.P. Zare, R.N. and Chandler, D.W. Science 260:1605-1610 (1993).
36. Blais, N.C. and Truhlar, D.G. *Chem. Phys. Lett.* 102:120-125 (1983); *J. Chem. Phys.* 83:2201-2206 (1985).
37. Charutz, D.M., Last, I., and Baer, M.*J. Chem. Phys.* 106:7654-7661 (1997).
38. Brownsword, R. A., Hillenkamp, M., Laurent, Th., Volpp, H.-R., Wolfrum, J., Vatsa, R. K., Yoo, and H.-S., *J. Phys. Chem. A*, 101:6448-6454 (1997).
39. Schatz, G.C., *Chem. Rev.* 87:81- 89 (1987).
40. Wrede, E., Schnieder, L., Welge, K. H., Aoiz, F. J., Banares, L., and Herrero, V. J., *Chem. Phys. Lett.* 265:129-136 (1997); Wrede, E., Schnieder, L., Welge, K.H., Aoiz, F. J. and Banares, L., Martínez-Haya, B., and Sáez Rábanos, V., *J. Chem. Phys.* 106:7862-7864 (1997).
41. Miller, J. A., *Twenty-Sixth Symposium (International) on Combustion*, The Combustion Institute, Pittsburgh, 1996, pp. 461-480.
42. Masten, D.A., Hanson, R.K., and Bowman, C.T., *J. Phys. Chem.* 94:7119-7128 (1990); Du, H. and Hessler, J. P., *J. Chem. Phys.* 96:1077-1092 (1992); Ryu, S. O., Hwang, S. M., and Rabinowitz, M.J., *J. Phys. Chem.* 99:13984-13991 (1995).
43. Seeger, S., Sick, V., Volpp, H.-R., and Wolfrum, J., *Israel J. Chem.* 34:5-18 (1994).
44. Miller, J.A., *J. Chem. Phys.* 74:5120-5132 (1981).
45. Kleinermanns, K. and Schinke, R., *J. Chem. Phys.* 80:1440-1445 (1984).
46. Varandas, A.J., *C. Mol. Phys.* 186:1159-1164 (1995).
47. Fei, R., Zheng, S.X. and Hall, G.E., *J. Phys. Chem. A* 101:2541-2545 (1997).
48. Kendrick, B., and Pack, R. T., *J. Chem. Phys.* 102:1994-2012 (1995).
49. Kendrick, B., and Pack, R. T., *J. Chem. Phys.* 106:3519-3539 (1997).
50. Koppe, St., Laurent , T., Volpp, H.-R., and Wolfrum, J., Naik, P. D., *Twenty-Sixth Symposium (International) on Combustion*, The Combustion Institute, Pittsburgh, 1966, pp. 489-495.
51. Kudla,K., Schatz, G.C. and Wagner, A.F., J. Chem. Phys. 95:1635-1647 (1991).
52. Clary, D.C. and Schatz, G.C., J. Chem. Phys. 99:4578-4589 (1993).
53. Balakrishnan, N. and Billing, G.D., *J. Chem. Phys.* 104:4005-4011 (1996).
54. Scherer, N. F., Khundkar, L. R., Bernstein, R. B., and Zewail, A.H., *J. Chem. Phys.* 82:1451-1453 (1987).
55. Ionov, S., Bruckner, G. A., Jacques, C., Valachovic, L., and Wittig, C., *J. Chem. Phys.* 97: 9486-9489 (1992); Jacques, C., Valachovic, L., Ionov, S., Böhmer, E., Wen, Y., Segall, J., and Wittig, C., *J. Chem. Soc. Faraday Trans.* 89:1419-1425 (1993).
56. Hoffmann, G., Oh, D., Chen, Y., Engel, Y. M., and Wittig, C., *Israel. J. Chem.* 30:115–129 (1990).
57. Kudla, K. and Schatz, G. C., in *The Chemical Dynamics and Kinetics of Small Radicals* (Liu, K. and Wagner, A. F., Ed.) World Scientific Publishing Co., 1994; Bowman, J. M.,and Schatz G. C., *Annu. Rev. Phys. Chem.* 46:169–195 (1995).
58. Schatz, G. C. and Dyck, *J. Chem. Phys. Lett.*, 188:11–15 (1992); Clary, D. C. and Schatz,G.C.,*J.Chem.Phys.*99:4578–458 9 (1994); Goldfield, E. M., Gray, S. K. and Schatz, G. C., *J. Chem. Phys.* 102:8807–8817 (1995).
59. Milligan, D. F. and Jacox, M. E., *J. Chem. Phys.* 54:927-942 (1971); Pettry, J. T., Harrison, J. A. and Moore, C. B., *J. Phys. Chem.* 97:11194-11198 (1993); Miyoshi, A., Matsui, H. and Washida, N., *J. Chem. Phys.* 100:3532–3539 (1994).
60. Kudla, K., Koures, A. G., Harding, L.B., and Schatz, G. C., *J. Chem. Phys.* 96:7465-7473 (1992).
61. Wooldridge, M. S., Hanson, R. K., and Bowman, C.T., *Int. J. Chem. Kinet.* 28:361-372 (1996); Wooldridge, M. S., Hanson, R. K., and Bowman, C. T., *Twenty-Fifth Symposium (International) on Combustion*, The Combustion Institute, Pittsburgh, 1994, pp. 741-748.
62. Rea, E. C. and Hanson, R. K., *Appl. Opt.* 22:518-520 (1983); Rea, E. C., Salimian, S. and Hanson, R. K., *Appl. Opt.* 23:1691-1694 (1984).
63. Arroyo, M. P., Langlois, S. and Hanson, R. K., *Appl. Opt.* 33:3296-3307 (1994); Philippe, L. C. and Hanson, R. K., *Appl. Opt.* 32:6090-6103 (1993).
64. Wehe, S. D., Baer, D. S. and Hanson, R. K., paper 97-3267 at the 33rd AIAA Joint Propulsion Conference Seattle, 1997.
65. Piepmeier, F. H., *Spectrochim. Acta B* 27:431 (1972); Daily, J. W., *Appl. Opt.* 6:568 (1977).
66. Fulle, D., Hamann, H. F., Hippler, H. and Troe, J., *J. Chem. Phys.* 105:983-1000 (1996).
67. Troe, J., *Twenty-Seventh Symposium (International) on Combustion*, The Combustion Institute, Pittsburgh, 1998.
68. Dreier, T. and Wolfrum, J., *Eighteenth Symposium (International) on Combustion*, The Combustion Institute, Pittsburgh, 1981, pp. 801-809.
69. Markus, M. W. and Roth, P., Proc. *Eigh-*

teenth Int. Symp. Shock Waves 2:1011-1018 (1992).
70. Dean, A. J. and Hanson, R. K., *Int. J. Chem. Kinet.* 24:517-532 (1992).
71. Fulle, D. and Hippler, H., *J. Chem. Phys.* 105:5423-5430 (1996).
72. Perry, R. A., *J. Chem. Phys.* 82:5485-5488 (1985).
73. Cooper, W. F. and Hershberger, J. F., *J. Phys. Chem.* 96:771-775 (1992); Cooper, W. F., Park, J., and Hershberger, J. F., *J. Phys. Chem.* 97:3283-3290 (1993).
74. Atakan, B. and Wolfrum, J., *Chem. Phys. Lett.* 178:157-162 (1991).
75. Mertens, J. D., Dean, A. J., Hanson, R. K., and Bowman, C. T., *Twenty-Fourth Symposium (International) on Combustion*, The Combustion Institute, Pittsburgh, 1992, pp. 701-709.
76. Becker, K. H., Kurtenbach, R., Schmidt, F., and Wiesen, P., *Ber. Bunsenges. Phys. Chem.* 101:128-133 (1997).
77. Flatness, S. A. and Kramlich, J. C., *Twenty-Sixth Symposium (International) on Combustion*, The Combustion Institute, Pittsburgh, 1996, pp. 567-573.
78. Pilgrim, J. S., Jennings, R. T., and Taatjes, C. A., *Rev. Sci. Instrum. 68* :1875-1878 (1997).
79. Pilgrim, J. S., McIlroy, A., and Taatjes, C. A., *J. Phys. Chem. A* 101:1873-1880 (1997).
80. Taatjes, C.A. and Daniel B.Oh., *Appl. Opt.* 36:5817-5821 (1997).
81. Howard, C.J. and Evensen, K.M., *Geophys. Res. Lett.* 4:437 (1977); Burrows, J.P., Cliff, D.I., Harris, G. W., Thrush, B. A., and Wilkinson, J.P.T., *Proc. Roy. Soc. London Ser A* 368:, 463 (1979); Hack, W., Preuss, A.W., Temps, F., Wagner, H.Gg., and Hoyermann, K., *Int. J. Chem. Kinet.* 12:851-860 (1980).
82. Carstensen, H.-H. and Wagner, H. Gg., *Ber. Bunsenges. Phys. Chem.* 99:1539- 1545 (1995).
83. Deters, R., Otting, M., Wagner, H. Gg., Temps, F., László, B., Dóbé, S. and Bérces, T., *Ber. Bunsenges. Phys. Chem.* 102:58-72 (1998).
84. Fridell, E., Westblom, U., Aldén, M. and Rosén, A., *J. of Catalysis* 128:92-98 (1991).
85. Gudmundson, F., Fridell, E., Rosén, A. and Kasemo, B., *J. Phys. Chem.* 97:12828-12834 (1993).
86. Langmuir, I., *Trans. Faraday Soc.* 17, 607-615 (1922).
87. Campbell, C.T. , Ertl, G. , Kuipers, H. , and Segner, J. , *J. Chem. Phys.* 73:5862-5873 (1980); Bär, C. , Zülike, M. Eiswirth, and Ertel, G., *J. Chem Phys.* 96: 8595-8604 (1992).
88. Freund, H.-J., *Ber. Bunsenges. Phys. Chem.* 99:1261-1281 (1995); Ertl, G., *Ber. Bunsenges. Phys. Chem.* 99:1282-1294 (1995).
89. Su. X. , Cremer, P. S. , Shen, Y. R., and Somorjai, G. A. , *J. Am. Chem. Soc.* 119: 3994-4000 (1997).
90. Brand, R.K. , Sorbollo, R.S., and Greenler, R.G., *Surf. Sci.* 271:605-615 (1992) 605
91. Ertl , G., in: *Catalysis Science and Technol.* 4 (Anderson, J. R. and Boudart, M., Eds.) Springer, New York, 1983 p. 209-282.
92. R. Kissel-Osterrieder, F. Behrendt, and J. Warnatz, *Twenty-Sventh Symposium (International) on Combustion*, The Combustion Institute, 1998.
93. Warnatz, J., *Eighteenth Symposium (International) on Combustion*, The Combustion Institute, Pittsburgh, 1981, pp. 369-381.
94. Frenklach, M., Wang, H., Goldenberg, M., Smith, G.P., Golden, D.M., Bowman, C.T., Hanson, R.K., Gardiner, W.C., Lissianski, V., Gas Research Institute Topical Report, Report No. GRI-95/0058, 1995.
95. Luque, J., Smith, G.P., and Crosley, D.R., *Twenty-Sixth Symposium (International) on Combustion*, The Combustion Institute, Pittsburgh, 1996, pp. 959-966; Luque, J. and Crosley, D.R., *Appl. Phys. B* 63:91-98 (1996); Juchmann, W. and Jeffries, J.B., *Appl. Opt.* 36:3261-3270 (1997).
96. Juchmann, W., Latzel, H., Shin, D.I., Peter, G., Dreier, T., Volpp, H.-R., Wolfrum, J., Lindstedt, R.P., and Leung, K.M., *Twenty-Seventh Symposium (International) on Combustion*, The Combustion Institute, Pittsburgh, 1998.
97. Scherer, J.J., Paul, J. B., O'Keefe, A., and Saykally, R.J., *Chem. Rev.* 97: 25-51 (1997).
98. Scherer, J.J. and Rakestraw, D.J., *Chem. Phys. Lett.* 265:169-176 (1997).
99. Scherer, J. J., Aniolek, K. W., Cernansky, N. P., and Rakestraw: D. J., *J. Chem. Phys.* 107:6196-6203 (1997); Scherer, J.J., Voelkel, D., and Rakestraw, D.J., *Appl. Phys. B* 64:699-705 (1997).
100. Reintjes, J. F., *Nonlinear Optical Parametric Processes in Liquids and Gases*, Academic Press, Orlando, 1984.
101. Eichler, H. J., Günter P., and Pohl, D. W., *Laser-induced dynamic Gratings*, Springer Series in Optical Sciences, Springer Verlag, Berlin, 1986.
102. R.A. Fisher Ed., Optical Phase Conjugation, Academic Press, New York, 1983.
103. Meacher, D.R., Charlton, A., Ewart, P., Cooper J., and Alber, G., *Phys. Rev. A* 42:3018-???? (1990).
104. Lucht, R. P., Farrow, R. L., and Rakestraw, D. J., *J. Opt. Soc. Am. B* 10:1508-1520 (1993).
105. Williams, S., Zare, R. N., and Rahn, L. A., *J. Chem. Phys.* 101:1093-1107 (1994).
106. Sick, V., Bui-Pam, M. N., and Farrow, R. L., *Opt. Lett.* 20:2036-2038 (1995).
107. Dreier, T. and Rakestraw, D., *Appl. Phys. B* 50:479-485 (1990); Germann, G. J., Mcll-

roy, A., Dreier, T., Farrow, R. L., and Rakestraw, D. J., *Ber. Bunsenges. Phys. Chem.* 97:1630-1634 (1993).
108. Vander Wal, R. L., Farrow, R. L., and Rakestraw, D. J., *Twenty-Fourth Symposium (International) on Combustion*, The Combustion Institute, Pittsburgh, 1992, pp. 1653-1659.
109. Tsay, S. J., Owens, K. G., Aniolek, K. W., Miller, D. L., and Cernansky, N. P., *Opt. Lett.* 20:1725-1727 (1995).
110. Smith, A. P., Hall, G., Whitaker, B. J., Astill, A. G., Neyer, D. W., and Delve, P. A., *Appl. Phys. B* 60:11-18 (1995).
111. Farrow, R. L. and Rakestraw, D. J., *Science* 257:1894-1900 (1992).
112. Germann, G. J., Farrow, R. L., and Rakestraw, D. J., *J. Opt. Soc. Am. B* 12:25-32 (1995).
113. Tanada, T. N., Velazques, J., Hemmi, N., and Cool, T. A., *Ber. Bunsenges. Phys. Chem.* 97:1516-1526 (1993).
114. Reichardt,T.A., Klassen, M.S., King, G.B., and Laurendau, N.M., *Appl. Opt.* 35:2125-2139 (1996).
115. Dreizler, A., Tadday, R., Monkhouse, P., and Wolfrum, J., *Appl. Phys. B* 57:85-87 (1993).
116. Agrup, S. and Aldén, M., *Chem. Phys. Lett.* 189:211-216 (1992); Agrup, S., Measurement of Quenched Fluorescence Lifetimes and Stimulated Emission from Flame Radicals, PhD Thesis, Lund Institute of Technology (1994), ISBN 91-628-1337-4.
117. Campbell, D.H., *Appl. Opt.* 23:1319-???? (1984).
118. Kienle, R., Lee, M. P., and Kohse-Höinghaus, K., *Appl. Phys. B.* 63:403-418 (1996).
119. Mailänder, M., *J. Appl. Phys.* 49:1256-1259 (1978).
120. Stepowski, D. and Cottereau, M.J., Progr. Astronaut. Aeronaut 95, (1989), pp. 642-657; Cottereau, M. J., *App. Opt.* 25:744-748 (1986).
121. Lucht, R.P., Sweeney, D.W., and Laurendeau N.M., *Appl. Opt.* 19:3295-3300 (1980).
122. Carter, C.D., King, G.B., and Laurendeau, N.M., *Appl. Opt.* 31:1511-1522 (1992).
123. Zizak, G., Petrucci, G.A., Stevenson, C.L., and Winefordner, J.D., *Appl. Opt.* 30:5270-5275 (1991).
124. Norton, T. S., Smyth, K. C., Houston Miller, J., and Smooke, M. D., *Combust. Sci. and Tech.* 90:1-34 (1993).
125. Smyth, K. C., *Combust. Sc. and Tech.*115:151-176 (1996).
126. Zizak, G., Lanauze, J., and Winefordner, J. D., *Appl. Opt.* 25:3242-3246 (1986).
127. Nyholm, K., Maier, R., Aminoff, C. G., and Kaivola, M., *Appl. Opt.* 32:919-924 (1993).
128. Löfstedt, B., Fritzon, R., and Aldén, M., *Appl. Opt.* 35:2140-2146 (1996).
129. Nyholm, K., Fritzon, R. and Aldén, M., *Opt. Lett.* 18:1672-1674 (1993).
130. Suvernev, A. A., Dreizler, A., Dreier, T., and Wolfrum, J., *Appl. Phys. B* 61:421-427 (1995).
131. Bockhorn, H., Fetting, F., Wannemacher, G., and Heddrich, A., *Ber. Bunsenges. Phys. Chem.* 91:819-825 (1987).
132. D'Alessio, A., Minutolo, P., Gambi, G., and D'Anna, A., *Ber. Bunsenges. Phys. Chem.* 97:1574-1582 (1993).
133. Minutolo, P., Gambi, G. and D'Alessio, A., *Twenty-Sixth Symposium (International) on Combustion*, The Combustion Institute, Pittsburgh, (1996), pp. 951-957.
134. McKinnon, J.T. and Howard, J.B. Twenty-Fourth *Symposium (International) on Combustion*, The Combustion Institute, Pittsburgh, (1992), pp. 965-971; Böhm, H., Feldermann, C., Heidermann, T. Jander, H. Lüers, B., and Wagner, H.Gg., *Twenty-Fourth Symposium (International) on Combustion*, The Combustion Institute, Pittsburgh, (1992), pp. 991-998.
135. Quay, B., Lee, T.-W., Ni, T., and Santoro, R. J., *Combust. Flame* 97:384-392 (1994).
136. Shaddix, C. R., Harrington, J. E., and Smith, K. C., *Combust. Flame* 99:723-732 (1994); 107:418-452 (1996).
137. Bengtsson, P.-E. and Aldén, M., *Appl. Phys. B* 60:51-59 (1995).
138. Vander Wal, R., Twenty-Sixth *Symposium (International) on Combustion*, The Combustion Institute, Pittsburgh, (1996), pp. 2269-2275.
139. Appel, J., Jungfleisch, B., Marquardt, M., Suntz, R., and Bockhorn, H., Twenty-Sixth *Symposium (International) on Combustion*, The Combustion Institute, Pittsburgh, (1996), pp. 2387-2395.
140. Regnier, P. R., and Taran, J.P.E., *Appl. Phys. Lett.* 23:240-242 (1973).
141. Péalat, M., Bouchardy, P., Lefebvre, M., and Taran, J. P. E., *Appl. Opt.* 24:1012-1022 (1985).
142. Lavorel, B., Millot, G., Bonamy, J., and Robert, D., *Chem. Phys.* 115:69-78 (1987).
143. Millot, G., Saint-Loup, R., Santos, S., Chaux, R., Berger, H., and Bonamy, J., *J. Chem. Phys.* 96:961-971 (1992).
144. Rahn, L. A., Farrow, R. L., and Rosasco, G. J., *Phys. Rev. A* 43:6075-6088 (1991).
145. Looney, J. P., Rosasco, G. J., Rahn, L. A., Hurst, W. S., and Hahn, J. W., *Chem. Phys. Lett.* 161:232-238 (1989).
146. Lavorel, B., Millot, G., Fanjoux, G., and Saint-Loup, R., *J. Chem. Phys.* 101:174-177 (1994).
147. Dreier, T., Ridder, M., Schiff, G., Saur, A., and Suvernev, A. A., *Twenty-Fifth Symposium (International) on Combustion*, The Combustion Institute, Pittsburgh (1994), pp 1727-1734.
148. Lavorel, B., Oksengorn, B., Fabre, D., Saint-Loup, R., and Berger, H., *Mol. Phys.*

75:397-413 (1992).
149. Moore, D. S., Schmidt, S. C., Shaw, M. S., and Johnson, J. D., *J. Chem. Phys.* 95:5603-5608 (1991).
150. Sala, J. P., Bonamy, J., Robert, D., Lavorel, B., Millot, G., and Berger, H., *Chem. Phys.* 106:427-439 (1986).
151. Koszykowski, M. L., Farrow, R. L., and Palmer R. E., *Opt. Lett.* 10:478-480 (1985).
152. Millot, G., Lavorel, B., Fanjoux, G., and Wenger, C., *Appl. Phys. B* 56:287-293 (1993).
153. Frank, E.U., *Pure and Appl. Chem.* 59:25-34 (1987); Steeper, R.R., Rice, S.F., Brown, M.S., and Johnston, S.C., *J. Supercrit. Fluids* 5:262-268 (1992).
154. Kychakoff, G. Howe, R.D., Hanson, R.K., and McDaniel, J.C., *Appl. Opt.* 21:3225-3227 (1982).
155. Dyer, M.J. and Crosley, D.R., *Opt. Lett.* 7:382-384 (1982).
156. Rothe, E.W. and Andresen, P., *Appl. Opt.* 36:3971-4033 (1997).
157. Heitzmann, T., Wolfrum, J., Maas, U., and Warnatz J., *Z. Phys. Chem. Neue Folge* 188:177-196 (1995).
158. Ketterle, W., Arnold, A., and Schäfer, M., *Appl. Phys. B* 51:91-93 (1990).
159. Gray, J. A. and Farrow, R. L. , *J. Chem. Phys.* 95:7054 (1991).
160 Heard, D. E. , Crosley, D. R., Jeffries,J. B., Smith, G. P., and Hirano, A. , *J. Chem. Phys.* 96:4366 (1992).
161. Doherty, P. M. and Crosley, D. R., *Appl. Opt. 23*, 713 (1984).
162. Rothe, E. W., Gu, Y., Chryssostomou, A., Andresen, P., and Bormann, F., *Appl. Phys. B* 66:251-258 (1998).
163. Arnold, A., Lange, B., Bouché,T., Heitzmann, T., Schiff, G., Ketterle, W., Monkhouse, P., and Wolfrum, J., *Ber. Bunsenges. Phys. Chem.* 96:1388-1393 (1992).
164. Dreizler, A., Sick, V. , and Wolfrum, J., *Ber. Bunsenges. Phys. Chem.* 101:771-782 (1997).
165. Bäuerle, B., Hoffmann, F., Behrendt F. and Warnatz, J., *Twenty-Fifth Symposium (International) on Combustion*, The Combustion Institute, Pittsburgh, 1994, pp. 135-141.
166. Warnatz, J. and Wolfrum, J., *Phys. Blätter* 47:193-200 (1991).
167. Warnatz, J., Maas, U., Dibble, R.W., Combustion, Springer, Heidelberg New York (1996).
168. Bray, K.N.C. *Twenty-Sixth Symposium (Inter national) on Combustion*, The Combustion Institute, Pittsburgh, 1996, pp. 1-26.
169. Nguyen, Q.-V., and Paul, P.H., *Twenty-Sixth Symposium (International) on Combustion*, The Combustion Institute, Pittsburgh, 1996, pp. 357-364.
170. Najm, H.N., Paul, P.H., Mueller, C.J., and Wyckoff, P.S., *Combust. Flame*, in press (1998).
171. Paul, P.H., and Najm, H.N., *Twenty-Seventh Symposium (International) on Combustion*, The Combustion Institute, Pittsburgh, 1998.
172. Masri, A.R., Dibble, R.W., and Barlow, R.S., *Prog. Energy Combust. Sci.* 22:307-362 (1996).
173. Drake, M.C., Bilger, R.W., and Stårner, S.H., *Nineteenth Symposium (International) on Combustion*, The Combustion Institute, Pittsburgh, 1982, pp. 459-467.
174. Dibbble, R.W., Kollmann, W., and Schefer, R.W., *Combust. Flame* 55:307-321 (1984).
175. Masri, A.R., Bilger, R.W., and Dibble, R.W., *Combust. Flame* 71:245-266 (1988).
176. Meier, W., Prucker, S., Cao, M.-H., and Stricker,W.,*Combust.Sci.Tech.*118:293-312 (1996).
177. Marran, D.F., Frank, J.H., Long, M.B., Stårner, S.H., and Bilger, R.W., *Opt. Lett.* 20:791-793 (1995).
178. Wehrmeyer, J.A., Cheng, T.-S., and Pitz, R.W., *Appl. Opt.* 29:2325-2332 (1990).
179. Brockhinke, A., Andresen, P., and Kohse-Höinghaus, K., *Appl.Phys.* B 62:533-545 (1995).
180. Nguyen, Q.V., Dibble, R.W., Carter, C.D., Fiechtner, G.J., and Barlow, R.S., *Combust. Flame* 105:499-510 (1996).
181. Stårner, S.H., Bilger, R.W.,Barlow, R.S., and Dibble, R.W., *Twenty-Third Symposium (International) on Combustion*, The Combustion Institute, Pittsburgh, 1990, p. 645-651.
182. Sanders, J.P.H., Gökalp, I., 8th International Symposium on Transport Phenomena in Combustion (1995).
183. Buschmann, A., Dinkelacker, F., Schäfer, T., and Wolfrum, J., *Twenty-Sixth Symposium (International) on Combustion*, The Combustion Institute, Pittsburgh, 1996, pp. 437-445.
184. Kelman, J.B. and Masri, A.R., *Appl. Opt.* 36:3506-3514 (1997); *Combust. Sci. Tech.* 129:17 (1997).
185. Bergmann,V., Meier, W., Wolff, D., and Stricker, W., *Appl. Phys. B*, accepted (1998).
186. Frank, J.H., Lyons, K.M., Marran, D.F., Long, M.B., Stårner, S.H., and Bilger, R.W., Twenty-Fifth *Symposium (International) on Combustion*, The Combustion Institute, Pittsburgh, 1994, pp. 1159-1166.
187. Yip, B.,Lam,J .K., Winter, M., and Long, M.B., Science 235:1209-1211 (1987).
188. Long, M.B., in Instrumentation for flows in combustion, Academic Press Ltd. pp.468-508 (1993).
189. Kremer, A., Landenfeld, T., Schäfer, T., Kazenwadel, J., Schulz, C., andWolfrum, J.,

Twenty-Seventh Symposium (International) on Combustion, The Combustion Institute, Pittsburgh, 1998.
190. Frank, J.H., Lyons, K.M., and Long, M.B., *Combust. Flame* 107:1-? (1996).
191. Carter, C.D., Donbar, J.M., and Driscoll, J.F., *Appl. Phys.* B 66, 129-132 (1998).
192. Long, M.B., Stårner, S.H., and Bilger, R.W., *Combust. Sci. and Tech.* 92:209-224 (1993)
193. Drake, M.C., French, D.T., and Fansler, T.D., *Twenty-Sixth Symposium (International) on Combustion*, The Combustion Institute, Pittsburgh, 1996, pp 2581-2587.
194. Tait, R. and Greenhalgh, D.A., *Ber. Bunsenges. Phys. Chem.* 97:1619-1625 (1993).
195. Großmann, F., Monkhouse, P. B., Ridder, M., Sick, V., and Wolfrum, J., *Appl. Phys.* B 62:249-253 (1996).
196. Lozano, A., Yip, B., and Hanson, R.K., *Exp. Fluids* 13:369-376 (1992).
197. Arnold, A., Buschmann, A., Cousyn, B., Decker, M., Vannobel, F., Sick, V., and Wolfrum, J., SAE Paper No. 932696, 1993.
198. Berckmüller, M., Tait, N.P., and Greenhalgh, D.A., SAE Paper No. 970826, 1997.
199. Yuen, L. S., Peters, J. E., and Lucht, R. P., *Appl. Opt.* 36:3271-3277 (1997).
200. Thurber, M. C., Grisch, F., and Hanson,R. K., Opt. Lett. 22:251 (1997).
201. Einecke,S., Schulz, C., and Sick, V., Laser Application to Chemical and Environmental Analysis, OSA Technical Digest Series (1998).
202. Melton, L.A. and Verdieck, J.F., *Twentieth Symposium (International) on Combustion*, The Combustion Institute, Pittsburgh, 1984, pp. 1283-1290; Melton, L.A., Ber. Bunsenges. Phys. Chem. 97:1560-1567 (1993).
203. Yeh, C.-N., Kamimoto, T., Kobori, S., and Kosaka, H., SAE Paper No. 932652, 1993.
204. Fröba, A.P., Rabenstein, F., Münch, K.-U., and Leipertz, A., *Combust. Flame* 112:199-209 (1998).
205. Grünefeld, G., Knapp, M., Beushausen, V., Andresen, P.,Hentschel, W., Manz, P., SAE Paper No. 952394, 1995; Knapp, M., Beushausen, V., Hentschel, W., Manz, P., Grünefeld, G., Andresen, P., SAE Paper No. 970827, 1997.
206. Espey, C., Dec, J.E., Litzinger, T.A., and Santavicca, D.A., Combust. Flame 109:65-86 (1997).
207. Winter, M. and Melton, L.A., *Appl. Opt.* 29:4574-4577 (1990).
208. Chang, R.K., in Advances in Laser Sciences II, American Institute of Physics, New York 1987, pp. 509-515.
209. Quian, S.-X., Snow, J.B., Tzeng, H.-M., and Chang, R.K., *Science* 231:486 (1986)
210. Swindal, J.C., Acker, W.P., Chen, G., Serpengüzel, A., and Chang, R.K.; in Recent Advances in Spray Combustion: Spray combustion Measurements and Model Simulation Vol II, AIAA, Reston, Virginia, 1995, pp. 63-90.
211. Bazile, R., and Stepowski, D., *Twenty-Fifth Symposium (International) on Combustion*, The Combustion Institute, Pittsburgh, 1994, pp. 363-370.
212. Le Gal, P., Farrugia, N., and Greenhalgh, D.A., *Opt. Lett.* (1998).
213. Schefer, R.W., Namazian, M., and Kelly, J., AIAA paper No. 87-1349 (1987).
214. Barker, D.B. and Fourney, M.E., *Opt. Lett.*, 1:135-137 (1977).
215. Reuss, D.L., Adrian, R.J., Landreth, C.C., French, D.T., and Fansler, T.D., SAE Paper No. 890616, 1989.
216. Adrian, R.J., *Annu. Rev. Fluid Mech.* 23:261-304 (1991).
217. Farugia, N., Kanne, S., and Greenhalgh, D.A., *Opt. Lett.* 20:1827-1829 (1995).
218. Stolz, W., Köhler, J., Lawrenz, W., Meier, F., Bloss, W.H., Maly, R.R., Herweg, R., and Zahn, M., SAE Paper No. 922354, 1992.
219. Komine, H. and Brosnan S.J., *Laser Anemometry* 1:273-277 (1991).
220. Miles, R.B. and Lempert, W.E., *Annu. Rev. Fluid Mech.* 29:285-326 (1997).
221. Boedecker, L.R., *Opt. Lett.* 14:473-475 (1989).
222. Miles, R.B., Connors, J., Markovitz, E., Howard, P., and Roth, G., *Phys. Fluids A* 1:389-393 (1989).
223. Bechtel, J.H., *Appl. Opt.* 18:2100 (1979).
224. Greenhalgh, D.A. 1990.
225. Farrow, R. 1990.
226. Dibble, R.W. and Hollenbach, R.E., *Eighteenth Symposium (International) on Combustion*, The Combustion Institute, Pittsburgh, 1981, pp.1489-1499.
227. Orth, A., Sick, V., Wolfrum, J., Maly, R.R., and Zahn, M., *Twenty-Fifth Symposium (International) on Combustion*, The Combustion Institute, Pittsburgh, 1994, pp. 143-150.
228. Schulz, C., Sick, V., Wolfrum, J., Drewes, V., Zahn, M., and Maly, R.R., *Twenty-Sixth Symposium (International) on Combustion*, The Combustion Institute, Pittsburgh,1996, pp. 2597-2604.
229. Forkey, J., Lempert, W.R., Bogdonow, S.M., Miles, R.B., and Russel, G., AIAA paper No. 94-0491.
230. Brugman, T.M., Klein-Douwel, R., Huigen, G., van Walwijk, E., ter Meulen, J., J. *Appl. Phys.* B 57:405-410 (1993).
231. Bräumer, A., Sick, V., Wolfrum, J., Drewes, V., Maly, R.R, Zahn, M., SAE Paper No. 952462, 1995.
232. Schulz, C., Yip, B., Sick, V., Wolfrum, J., *Chem. Phys. Lett.* 242:259-264 (1995)
233. Schulz, C., Sick, V., Wolfrum, J., Drewes, V., Zahn, M., Maly, R.R., *Twenty-Sixth Symposium (International) on Combustion*, The Combustion Institute, Pittsburgh,1996, pp. 2597-2604.

234. Knapp, M., Luczak, A., Beushausen, V., Hentschel, W., Manz, P., Andresen P., SAE Paper No. 970824, 1997.
235. Hildenbrand, F., Schulz, C., Sick, V., Josefsson, G., Magnusson, I., Andersson, Ö., Aldén, M., SAE Paper No. 981047, 1998.
236. DiRosa, M.D., Hanson, R.K., *J. Quant. Spectrosc. Radiat. Transfer* 52:515-529 (1994).
237. Schulz, C., Sick, V., Heinze, J., Stricker, W., *Appl. Opt.* 36:3227-3232 (1997).
238. Paul, P.H., Gray, J.A., Durant Jr., J.L., Thoman Jr., J.W., *Appl. Phys. B* 57:249-259 (1993).
239. Paul, P.H., Gray, J.A., Durant Jr., J.L., Thoman Jr., J.W., AIAA Journal 32:1670-1675 (1994).
240. Furlanetto, M.R., Thoman Jr., J.W., Gray, J.A., Paul, P.H., Durant Jr., J.L., *J. Chem. Phys.* 101:10452-10457 (1994).
241. Schulz, C., Wolfrum, J., Sick, V., *Twenty-Seventh Symposium (International) on Combustion*, The Combustion Institute, Pittsburgh, 1998.
242. Meier, U., in final report JOF3-CT95-0025 CEC Research Contract, in press (1998).
243. Kaminski, C.F., Engström, J., Aldén, M., *Twenty-Seventh Symposium (International) on Combustion*, The Combustion Institute, Pittsburgh, 1998.
244. Josefsson, G., Magnusson, I., Hildenbrand, F., Schulz, C., Sick, V., *Twenty-Seventh Symposium (International) on Combustion*, The Combustion Institute, Pittsburgh, 1998.
245. Beér, J.M.,Twenty-Second Symposium (International) on Combustion, The Combustion Institute, Pittsburgh, 1988, pp. 1-16
246. Trushin, S.A., *Ber. Bunsenges. Phys. Chem.* 96, 319-322(1992).
247. Cheo, P.K., Zhiping, C., Li, C., and Yi, Z., *Appl. Opt.* 32, 836-841 (1993)
248. Cooper, D.E., and Gallagher, T.F., *Appl. Opt.* 24, 710-716 (1985)
249. Meienburg, W., Neckel, H., Wolfrum, J.: Twenty-Third Symposium (International) on Combustion, The Combustion Institute, Pittsburgh, 1990, pp. 231-236
250. Arnold, A., Becker, H., Hemberger, R., Hentschel, W., Ketterle, W., Köllner, M., Meienburg, W., Monkhouse, P., Neckel, H., Schäfer, M., Schindler, K.P., Sick, V., Suntz, R., Wolfrum, J., *Appl. Opt.* 29, 4860-4872 (1990)
251. Tsuboi, T., Arimitsu, N., Ping, D., and Hartmann, J.M., *Jpn. J. Appl. Phys.* 24: 8-13 (1985)
252. Emrich, R.J., Soloukhin, R.I. *Astronautica Acta* 17: 639 (1972)
253. Mallard, W.G. and Gardiner, W.C., *J. Quant. Spectrosc. Radiat. Transfer* 20: 135-149 (1978)
254. Mongia, R.K., Tomita, E., Hsu, F.K., Talbot, L., and Dibble, R.W., Twenty-Sixth Symposium (International) on Combustion, The Combustion Institute, Pittsburgh, 1996, pp. 2749-2755
255. Furlong, E.R., Baer, D.S., and Hanson, R.K., Twenty-Sixth Symposium (International) on Combustion, The Combustion Institute, Pittsburgh, 1996, pp. 2851-2858
256. Mihalcea, R.M., Baer, D.S., and Hanson, R.K., *Appl. Opt.* 36, 8745-8752 (1997)
257. Mihalcea, R.M., Baer, D.S., and Hanson, R.K., paper no. AIAA 97-3356, 33rd AIAA Joint Propulsion conference ; July 6-9, 1997 Seattle, WA, USA
258. Gopual, N.K.J.M., Newfield, M.E., Baer, D.S., and Hanson, R.K., *Opt. Lett.* 19: 1900-1902 (1994)
259. Ebert, V., Fitzer, J.,Gerstenberg, I., Pleban, K.-U., Pitz, H., Wolfrum, J., Jochem, M., Martin, J., submitted to Twenty-Seventh Symposium (International) on Combustion,, August 2-7, 1998, Boulder, CO, USA
260. Kessler, W.J., Sonenfroh, D.M., Upschulte, B.L., and Allen, M.G., paper no. AIAA 97-2706, 33rd AIAA Joint Propulsion conference ; July 6-9, 1997 Seattle, WA, USA
261. Wandt, D., Laschek, M., Tünnermann, A., and Welling, H., *Opt. Lett.* 22: 390-392 (1997)
262. Wandt, D., Laschek, M., Przyklenk, K.,Tünnermann, A., and Welling, H., *Opt. Comm.* 130: 81-84 (1996)
263. Larson, A.P., Sandstrom, L., Hojer, S., Ahlberg, H., and Broberg, B., *Opt. Eng.* 36: 117-123 (1997)
264. Sonenfroh, D.M., Upschulte, B.L., and Allen, M.G., paper at OSA LACEA(Laser Appl. to Chem. Envir. Analysis) 8-11 March, 1998, Orlando, FL, USA
265. Nagali, V., Hanson, R.K., *Appl. Opt.* 36: 9518-9527, (1997)
266. Komine, H., Brosnan, S.J., Litton, A.B., and Staperts,E.Q., paper no AIAA 91-0337, 29th Aerospace Sciences Meeting, Reno, Nev. 7-10 January 1991
267. Miles, R.B., Lempert, W.R., Appl. Phys. B 51:1-7 (1990)
268. Smith, M.W., Northam, G.B., 33rd Aerospace Sciences Meeting, Reno, Nev., 9-12 January, 1995
269. Shirley, J.A., Winter, M., 31st Aerospace Sciences Meeting, Reno, Nev., 11-14 January, 1993
270. Miller, M.F., Kessler, W.J., and Allen, M.G., *Appl.Opt.* 35, 4905-4912, (1996)
271. Ritter, K.J., Wilkerson, T.D., J. Mol. Spec. 121: 1-19 (1987)
272. Philippe, L.C., and Hanson, R.K., *Opt. Lett.* 16: 2002-2004 (1991)
273. Philippe, L.C., and Hanson, R.K., *Appl. Opt.* 32: 6090-6103 (1993)
274. Furlong, E.R., Mihalcea, R.M., Webber, M.E., Baer, D.S., Parr, T.P. and Hanson,

R.K., paper no AIAA 97-2833 at the 33rd Joint propulsion conference, July 6-9, 1997, Seattle, WA
275. Schuler, F., Rampp, F., Martin, and J., Wolfrum, J., Combustion and Flame 99: 431-439 (1994)
276. Ebert, V., Sick V., J. Wolfrum, Technisches Messen 63 7/8, 268-277 (1996) (in german)
277. Oldenburg, R.C., Baughcum, S.L., *Anal. Chem.* 58: 1430-1436 (1986).
278. Helble, J.J., Srinivasachar, S., Ham, D.O., Boni, A.A., Charon, O., Modestino, A., *Comb. Sci. Tech.* 81: 193-205 (1992).
279. Hartinger, K.T., Monkhouse, P.B., Wolfrum, J., Baumann, H., Bonn, B., *25th Symp. (Inter-national) on Combustion.* The Combustion Institute, Pittsburgh, 1994, pp. 193-199.
280. Chadwick, B., Domazetis, G., Morrison, R.J.S., *Anal. Chem.* 67: 710-717 (1995).
281. Greger, F., Hartinger, K.T., Monkhouse, P.B., Wolfrum, J., Baumann, H., Bonn, B., *26h Symp. (International) on Combustion.* The Combustion Institute, Pittsburgh, 1996, pp. 3301-3307.
282. Hartinger, K.T., Nord, S., Monkhouse, P.B., Appl. Phys. B, 64: 363-367 (1997).
283. Buckley, S.G., McEnally, C.S., Sawyer, R.F., Koshland, C.P., Lucas, D., *Combustion Sci. Technol.* 118: 169-188 (1996).
284. Hernberg, R.G., Häyrinen, V.T., , in "High Temperature Gas Cleaning", E. Schmidt, P. Göng, T. Piltz, A. Dittler, (eds.), Institut für Mechanische Verfahrenstechnik & Mechanik der Universität Karlsruhe, Karlsruhe, Germany , (1996) pp. 694-705.
285. Jäglid, U., Olsson, J.G., Pettersson, J.B.C., *J. Aerosol Sci.* 26: 637-638 (1995); 27 (1996) 967-977; Olsson, J.G., Jäglid, U., Pettersson, J.B.C., *Energy & Fuels* 11: 779-784 (1997).